Observational evaluation of outdoor cooling potential of air-source heat pump water heaters

Kazuki Yamaguchi (yamaguchi.ka@tepco.co.jp)
Tokyo Electric Power Company Holdings, Inc. https://orcid.org/0000-0001-6478-9336
Tomohiko Ihara
The University of Tokyo
Yukihiro Kikegawa
Meisei University

Research Article

Keywords: Air-source heat pump water heater, Cold exhaust, Urban heat island, Building-scale climate, Observation

Posted Date: March 2nd, 2021

DOI: https://doi.org/10.21203/rs.3.rs-255294/v1

Observational evaluation of outdoor cooling potential of air-source heat pump water heaters

Kazuki Yamaguchi [1,*], Tomohiko Ihara [2], Yukihiro Kikegawa [3]

[1] TEPCO Research Institute, Tokyo Electric Power Company Holdings, Inc., 4-1 Egasaki-cho, Tsurumi-ku, Yokohama, Kanagawa 230-8510, Japan
[2] Graduate School of Frontier Sciences, The University of Tokyo, 5-1-5 Kashiwanoha, Kashiwa, Chiba 277-0882, Japan
[3] School of Science and Engineering, Meisei University, 2-1-1 Hodokubo, Hino, Tokyo 191-8506, Japan

* Corresponding author. E-mail address: yamaguchi.ka@tepco.co.jp (K. Yamagcuhi).

Abstract

Heat pump water heaters are highly efficient hot water supply systems that effectively utilize the heat of outdoor air via heat pump technology. Many studies have been conducted to optimize the design and operation of heat pump water heaters from the perspective of climate change mitigation. Air-source heat pump water heaters, which absorb heat from the outdoor air and emit cold exhaust, can also be expected to alleviate the urban heat island effect; however, this has not been studied extensively. To estimate the impact of cold exhaust on building-scale climate, we conducted a multipoint measurement of the outdoor thermal environment around a low-rise apartment building equipped with air-source heat pump water heaters, in both summer and winter. Observations showed a substantial cooling effect that decreased air temperatures by 1 °C within the site boundary on summer nights when multiple heat pump water heaters operated concurrently. The analysis revealed that the sensitivity of the ambient temperatures to cold exhaust depends strongly on local atmospheric conditions. The most influential factor was the wind direction: the sensitivity increased significantly when the exhaust outlet location was at the lee side of the building. Naturally, the wind speed also affected the sensitivity, which tended to be higher when the wind speed was lower. The convective stability near the ground surface, however, showed no significant influence over the sensitivity.

Keywords:

Air-source heat pump water heater, Cold exhaust, Urban heat island, Building-scale climate, Observation

Declarations

Funding

This research did not receive any specific grant from funding agencies in the public, commercial, or not-for-profit sectors.

Conflicts of interest/Competing interests

The authors declare that they have no known competing financial interests or personal relationships that could have appeared to influence the work reported in this paper.

Availability of data and material

Not applicable

Code availability

Not applicable

1 Introduction

According to IPCC AR4 WG2 (2007), it is now clear that mitigation alone cannot prevent the effects of climate change. Thus, the international community is promoting both mitigation and adaptation as ways to combat climate change. In particular, urban areas, which consume a large amount of energy, suffer from the combined impact of global warming and the urban heat island (UHI) effect. A balanced combination of measures consisting of mitigation and adaptation is required to tackle this issue.

Water heating accounts for a large percentage of total energy consumption in the domestic sector, estimated at 14% in the US (IEA 2018), 16.8% in the UK (BEIS 2019), and 29.1% in Japan (ANRE 2019); it is also a major source of CO_2 emissions. The air-source heat pump water heater (ASHPWH) system is a highly efficient hot water supply device that employs heat pump technology to effectively utilize the heat of outdoor air. This is a technology expected to contribute to the mitigation of climate change by reducing CO_2 emissions.

The performance of ASHPWH systems is affected by characteristics of the external environment, such as outdoor air temperature and supply water temperature. Morrison et al. (2004) showed that according to experiment-based seasonal performance assessments, air temperature had a greater impact than water temperature. Yokoyama et al. (2007) noted that, according to numerical simulations, outdoor air temperatures have a significant impact on system efficiency and energy consumption. Guo et al. (2011) conducted model simulations to improve design and operational optimization in terms of the thermal and economic performance. Their results showed that the optimal starting time is determined by the difference in the unit cost of electricity between day and night, but the optimal setting water temperature is determined according to the seasonal change in the outdoor air temperature.

ASHPWH systems are less suitable for cold climates because low outdoor temperatures lead to reduced efficiency (Singh et al. 2010); however, field experiments in the northeastern and northwestern parts of the United States have shown that the system coefficient of performance (COP) reaches 1.5–2.6 (Shapiro and Puttagunta 2010; Ecotope and NEEA 2015). This means a 40–65% reduction in secondary energy consumption compared to a conventional electric water heater or a gas water heater with thermal efficiencies of around 0.9. Further improving the performance of air-source heat pumps (for space or water heating) at low temperatures has been a major focus in recent years, and numerous research studies have been carried out (e.g., Tello-Oquendo et al. 2019; Kim et al. 2019; Wei et al. 2020a, b).

One problem with heat pump water heaters is that hydrofluorocarbons (HFCs), which are used as refrigerants, have an extremely high global warming potential (GWP). Therefore, considering HFC leakage, it has been calculated that the lack of adequate performance in cold climates can lead heat pump water heaters to have the same environmental impact, in terms of greenhouse gas emissions, as gas water heaters (Johnson 2011). Thus CO_2, which has a low GWP and performs excellently as a refrigerant, has been attracting attention as a possible replacement for HFCs. Nekså et al. (1998) showed that a prototype heat pump water heater using CO_2 as a refrigerant yielded an annual average COP of around 4, even under climatic conditions in Oslo. In addition, an investigation by Cecchino et al. (2005) using a simulation showed that the COP of CO_2-ASHPWH systems could reach between 4 and 5 in winter (with an outdoor air temperature of 10 °C) and between 7 and 9 in summer (with an outdoor air temperature of 30 °C).

There have been many studies focused on the dependency of COP, and other associated parameters, on outdoor air temperature; this is to optimize the design and operation of ASHPWH systems. This is done mainly from the viewpoint of climate change mitigation. However, the impact of the operation of ASHPWHs on outdoor air temperatures has not attracted as much attention. In theory, ASHPWHs

can contribute to the alleviation of the UHI, explained as follows.

(1) In order to obtain a heat output of 100, a conventional gas-fired or electric water heater with a thermal efficiency of around 0.8 requires 125 units of combustion energy, and ultimately emits 125 units of heat (Fig. 1a). In contrast, an ASHPWH with a COP of around 4 requires 25 units of electrical energy and 75 units of external thermal energy from outdoor air, and emits a net value of 25 heat units (100 hot combined with 75 cold units as shown in Fig. 1b). Thus, ASHPWHs can greatly reduce heat emission compared to conventional gas/electric water heaters.

(2) Cold exhaust from the outdoor units of ASHPWHs does not diffuse easily since it is on average several degrees Celsius cooler than the ambient temperature, and it therefore tends to sink. Thus, its effect on the air temperature at ground level can be significantly greater than that from hot exhaust. In addition, the cold exhaust occurs at night when the atmosphere is more stable and has an enhanced cooling effect compared to that observed during daytime. Therefore, even if the net heat emission is positive, the cooling effect of the cold exhaust greatly exceeds the effect of the hot exhaust.

(3) While a significant portion of the heat from waste water would be conveyed far from the residential area in the city, cold exhaust is emitted on site. If we assume the residential area as the system boundary, it can be considered that ASHPWHs recover excess heat within the system and eventually dump the recovered heat out of the system.

The UHI has various impacts such as increased energy consumption for cooling and increased likelihood of heat strokes among people. Heat stroke tends to be more severe at night because people are unaware of the early symptoms of heat stroke during sleep. In 2019, about half of the heat stroke deaths in Tokyo's 23 wards occurred at night (Bureau of Social Welfare and Public Health 2019). Furthermore, the sleep disorders caused by the high temperatures at night have a particularly significant impact on human health (Nastos and Matzarakis 2008; Ihara et al. 2015; van Loenhout et al. 2016; Obradovich et al. 2017). In general, the use of air-conditioning is an effective measure for adapting to indoor thermal environments (Karkour et al. 2021). However, nighttime health hazards have become a serious problem, even in the urban residential areas of Tokyo, where use of air-conditioning is widespread. Many mega-cities in tropical developing countries have low air-conditioning penetration rates in their residences (IEA 2018), and there are concerns that the increase in nighttime temperatures associated with progressive urbanization will cause more serious health problems. As an adaptive measure to such health hazards, the widespread use of air-conditioning alone is insufficient, and measures to reduce outdoor temperatures at night are necessary.

Increasing the albedo of city surfaces or installing vegetated green surfaces are promising measures for alleviating the UHI, and many studies have been conducted to evaluate their effects (e.g., Rosenfeld et al. 1995; Savio et al. 2006; Synnefa et al. 2008; Chen et al. 2009; Zhou and Shepherd 2010; Ng et al. 2012). However, although these measures are effective in lowering daytime temperatures, their effects on nighttime temperatures are limited. Santamouris (2012) reviewed several simulation studies and showed that when the albedo of city surfaces is globally increased, the expected mean decrease in the average ambient temperature is approximately 0.3 °C per 0.1 rise in albedo, and the corresponding average decrease of the peak ambient temperature is approximately 0.9 °C. Similarly, the average and peak values for cool roofs were 0.2 °C and 0.41 °C (per 0.1 rise in albedo), respectively; for green roofs, the average and peak values range from 0 (negligible)–0.55 °C and 0–0.86 °C, respectively. Because the peak values appear during the day, the corresponding values at night are smaller than the average values, suggesting the difficulty of lowering the outdoor temperature at night.

Given the abovementioned background, the effectiveness of the ASHPWH as a measure of nighttime UHI should be verified. The use of ASHPWHs to lower nighttime outdoor temperatures and

to curtail the negative impacts of the UHI is a potential adaptation measure for climate change. In this case, the design and operation of ASHPWHs may be optimized in terms of both mitigation and adaptation to climate change. However, few studies have evaluated ASHPWHs as an adaptation measure.

Anthropogenic heat, artificial ground surfaces, and urban morphology have long been considered and studied as the three primary factors causing the UHI. It is known that the impact of these factors on city temperatures varies with time and season, and that anthropogenic heat contributes greatly to the rise of temperatures at night and in winter (Atwater 1972; Ichinoise et al. 1999; Kusaka and Kimura 2004; Fan and Sailor 2005; Ryu and Baik 2012). Kimura and Takahashi (1991) conducted an experiment using a regional climate model and found that anthropogenic heat has contributed to an increase in surface temperatures in the Tokyo metropolitan area of 1 °C during the day and 2−3 °C at night. Ohashi et al. (2007) used observations and simulations to compare the outdoor air temperatures during weekdays and holidays in office districts in central Tokyo and showed that temperatures during the summer were 1−2 °C higher due to heat exhaust from air conditioners. As the impacts of anthropogenic heat on urban temperatures also depends on urban morphology, studies on this have also been conducted using computational fluid dynamics (CFD) simulation (e.g., Adelia et al. 2019).

However, these studies are aimed at hot exhaust, which has higher temperatures than that of ambient air. No previous research has been conducted on the effects of "cold exhaust," which is lower in temperature than ambient air, through observational measurement or numerical simulations. While studies concerning anthropogenic heat focus on the impact at various scales, from mesoscale to city-block scale, the impact of cold exhaust at the broad-area scale has drawn little attention since the ASHPWH, its emission source, is not yet widespread. Considering prospects for the spread of the ASHPWH in the future, however, it would be meaningful to examine its outdoor cooling potential by building scale observation. In this study, measurements of the thermal environment were taken around a low-rise residential apartment building equipped with ASHPWHs.

The cooling effect can be concluded directly in accordance with the law of conservation of energy. As the ASHPWH absorbs heat from the ambient air around the target building, temperature reductions in the ambient air are likely. The research has the following two main objectives:

(1) To quantitatively measure the thermal environment at the building scale under actual uncontrolled ASHPWH operating conditions.

(2) To qualitatively analyze and identify meteorological factors that influence the effect of temperature reduction to achieve an approximate understand how the cooling effect depends on local atmospheric conditions, such as wind direction, wind speed, and thermal convection.

For the first objective, confirming that the temperature drops by approximately 0.1−1 °C—which is comparable to the daytime peak effect of cool and green roofs (Santamouris, 2012)—would justify conducting further detailed studies and position ASHPWH as a promising countermeasure to the nighttime UHI. Regarding the second objective, the measurements conducted on a real house in this study have many constraints and a large degree of uncertainty. To conduct a quantitative analysis of the relationship between the amount of exhaust heat, local atmospheric conditions, and temperature reduction, experiments in a controlled environment are necessary. Such a quantitative analysis will be the focus of subsequent studies, after the objectives of this study are achieved.

2 Methods and conditions

2.1 Outline of the measurement

We selected a low-rise apartment building in Shinjuku Ward, Tokyo, as our target building (Fig. 2).

It is built of reinforced concrete with three floors aboveground (10.0 m height). The site has an area of 910 m^2 (40.9 m × 22.3 m), of which the building occupies 230 m^2 (27.5 m × 8.4 m), and the total floor space is 630 m^2. It accommodates 16 households, with an average occupied area of about 30 m^2 per household; 12 of these are single-occupancy, while the other 4 are double-occupancy. The occupants were not informed about the purpose of the observation to avoid influencing their hot water usage. A CO_2-ASHPWH (Corona, CHP-452) is installed in each apartment. A total of 12 outdoor units were placed in four vertical rows (columns #1–4) by three horizontal rows (top, middle, and ground floors) on the northern side of the building; the other four units were placed in two columns (#5 and #6) by two rows (top and middle floors) on the southern side. The site is surrounded by 2-m high fences. The northern and southern boundaries have blindfolded fences with no openings, whereas the eastern and western boundaries have mesh fences with an opening ratio of approximately 90%.

The observation periods were August 20–September 10, 2008 for summer and February 15–25, 2011 for winter. To measure the temperature of the outdoor air, thermistor thermometers (T&D, RTR-52) fitted with solar shields were used. To capture the horizontal distribution of temperatures at a height of 1.5 m, three measurement points were set on the eastern, southern and northern sides of the site, and two points were set on the western side (Fig. 2a). In particular, the three measurement points on the northern side (N-1, N-2, and N-3) were located at the midpoints of the adjacent vertical rows of exhaust outlets and as far from the outlets as possible to avoid the direct impact of cold exhaust before it diffuses. In addition, to capture the vertical structure of temperature, 7 measurement points were set at 0.5 m and 5 points were set at heights of 2.8 m, 5.5 m, and 8.2 m, each positioned 0.3 m from the north-side wall (Fig. 2b) during the summer observation period. Ground surface temperatures (T_g) were measured at two points on the concrete pavement in the northern side of the site (Fig. 2a) using type-T thermocouple wires (Onset, TCW100-T), and the averaged values are used for the analysis. General weather conditions including air temperature (T_a), wind speed and wind direction were measured by a weather station (Davis, Vantage Pro2) installed 1.5 m from the surface of the roof, i.e., 11.5 m above the ground. The data measurement interval for the thermistor thermometer was set to 30 s, the thermocouple was set to 1 min, the weather station was set to 10 min, and the average value over 10 min was used while analyzing the results. Each thermistor thermometer was calibrated using an Assmann ventilated psychrometer (Sato Keiryoki Mfg., SK-RHG-S), and the measured values were corrected using the relevant calibration formula.

Since we conducted the investigation in an occupied house, not an experimental location, the need for privacy for the occupants meant there were several limitations on taking measurements. Since only a few instruments could be placed discreetly within the site, detailed airflow data around the building could not be obtained. A further limitation stems from the nature of ambient air. If it was trapped in a certain area, it could act as a control so that we could determine the exact temperature drop. However, ambient air normally flows in many different directions, which made it difficult to measure the exact drop in temperature. In addition, energy-related data such as usage and schedules were not directly available for this study.

2.2 Cold exhaust profile

In order to evaluate the impact of the exhaust heat on outdoor air temperature, it is essential to know when and how much it is emitted. The ASHPWH is a thermal storage system that always operates at a rated load at a set time, regardless of the hot water consumption schedule. In order to minimize heat loss from the storage tank, and to simultaneously take advantage of the cheaper electricity rates offered at night, the system is usually pre-programmed to run from late night to early morning. Its operating time and the quantity of cold exhaust vary by season. The total amount of exhaust heat H_n [kW] from multiple water heater units can be estimated based on the heating capacity

Q [kW/unit], energy consumption E [kW/unit], and number of operating units n [units] using the following equation:

$$H_n = (E - Q)n. \quad (1)$$

In the case of the ASHPWH (with larger Q than E), H_n has a negative value indicating the amount of heat energy absorbed from outdoor air. Because the actual heating capacity and energy consumption could not be measured in this study, the rated values specified by the manufacturer were used to set Q at 4.5 throughout the year and to estimate E as a function of outdoor temperature (Eq. 4 in Appendix A). The air temperature T_a measured on the rooftop (described in the next section) was used as the outdoor temperature. The value of n was determined based on records of thermistor thermometers installed near the exhaust outlets of the outdoor units (Fig. 3). Because the temperature of the cold exhaust was approximately 7 °C below the ambient air temperature, the on/off status of each unit could be clearly determined. Of the 16 units on the site, the 12 units on the northern side of the building were targeted for monitoring, whereas the four units on the southern side were placed in private areas of the estate and not monitored in this study.

The results of the monitoring revealed that each unit operates at approximately the same time for each season (Fig. 4). Overall, the units primarily ran from 4:00–6:30 am in the summer and from 1:30–6:30 am in the winter. The winter duration is approximately two times longer than the summer duration, primarily because the input water temperature is lower in winter, requiring more energy to heat the water to the same temperature. Because each unit was operated on a pre-programmed schedule, the observed day-to-day variations in the number of active units were small. The average number of operating units n peaked at 7.1 at 5:30 am in the summer and at 9.4 at 4:10 am in the winter. Units T-1, M-3, and M-4 in the summer and T-1 and G-2 in the winter either operated infrequently or were out of operation. The large number of single-occupancy apartments in the target building likely caused a lower demand for hot water than that of a standard household. Figure 5 shows the estimated average total amount of H_n over time during each observation period. H_n was nearly proportional to n—despite also depending on the outdoor temperature—with a peak value of −24.2 at 5:30 am in the summer and −30.4 at 4:10 am in the winter. The average daily integrated values of H_n for summer and winter reach −123.9 and −242.4 kJ, respectively. If the total amount of the cold exhaust stayed in the space within a 10-m height of the site (6802 m^3 excluding the volume of the building), it could cause temperature drops of 15.3 and 28.2 °C in summer (when the outdoor temperature is 25 °C) and winter (when the outdoor temperature is 7 °C), respectively. In practice, under calm conditions, the cold exhaust assumedly sinks downward and spreads to more gently cool a wider area closer to the ground.

Owing to the limited number of measurement points, part of the exhaust was advected and diffused outside the site and did not affect the observed air temperature. The horizontal and vertical distribution of multiple exhaust outlets is one of the primary factors that make it difficult to evaluate the temperature sensitivity to cold exhaust in this study. In general, higher exhaust outlet locations closer to the boundary in the horizontal direction leads to greater advection diffusion out of the target area and a smaller temperature effect within the area. Additionally, the cold exhaust from the four units on the southern side of the building were not monitored, providing another uncertainty that makes the evaluation difficult. To minimize the influence of cold exhaust from the south side, only three measurement points on the northern side (N-1, N-2, and N-3) were considered for the temperature sensitivity evaluation. The results of the CFD evaluation showed that under calm conditions, the cold exhaust from the middle and top floors registered 44% and 32% of the temperature effect of the ground floor, respectively; the cold exhaust from the outer two columns registered 91% of the temperature effect of the inner two columns (Appendix B). Here, we introduce an index of the effective amount of cold exhaust H_e, which is obtained by multiplying the total amount of cold exhaust H_n [kW] by a coefficient that considers the difference in temperature effects due to the location of the

exhaust outlet as:

$$H_e = [(n_G + 0.44n_M + 0.32n_T)/n][(n_I + 0.91n_O)/n]H_n \ (n > 0), \quad (2)$$

where n_G, n_M, and n_T are the numbers of operating units on the ground floor, middle floor, and top floor, respectively; and n_I and n_O are those in the inner (#2 and # 3) and outer (#1 and #4) columns. Figure 5 shows that the pattern of the time variation of the average H_e for each observation period is nearly proportional to that of H_n for each period, with a peak value of −16.1 at 5:30 am in summer, and −16.0, at 4:10 am in winter.

2.3 Weather overview

The air temperatures measured at the rooftop (T_a) were shown in Fig. 6. During the observation period for summer 2008, it was relatively cool and there were only four tropical nights (nights with a minimum temperature of 25 °C or higher), mainly due to the unstable atmosphere caused by low pressure and weather fronts in late August. The average daily minimum temperature for each observation period of summer and winter was approximately 23.1 °C and 4.6 °C, respectively.

In this study, we grouped wind directions into two main directions: north (from WNW to ENE) and south (from ESE to WSW). Observations of the wind direction distribution showed that northerly winds were dominant when the ASHPWHs were in operation (Fig. 7). In particular, no southerly wind days were observed during the winter observation period. When the wind speed, air temperature (T_a), and ground surface temperature (T_g) are averaged by main wind direction for each observation period (Table 1), the following trends were observed. During the summer observation period, compared to the northerly wind days, the southerly wind days were much calmer and hotter by about 3 °C. The convective stability near the ground surface can be roughly estimated based on the difference between T_a and T_g. It was in a nearly neutral state on the southerly wind days ($T_g - T_a$ = 0.0 °C), while it was unstable on the northerly wind days ($T_g - T_a$ = 2.9 °C). These observations confirm that the UHI is more intense under calm and stable atmospheric conditions. On the northerly wind days in winter, the average wind speed was at par with that of northerly wind days in summer; however, it was rather stable ($T_g - T_a$ = −1.7 °C) in terms of convective state near the ground surface.

2.4 Quantification of the cooling effects

While quantifying the temperature decrease due to cold exhaust from ASHPWHs, the measured air temperature on the rooftop (T_a) was set as the baseline on the assumption that it is not affected by the cold exhaust. Biases were removed for the air temperature at each measurement point so that the average value during the period when the ASHPWHs did not operate (0:00–3:00 am for summer and 23:00 pm–0:00 am for winter) was equal to the rooftop air temperature. The deviation from the rooftop air temperature (ΔT) at each measurement time was regarded as being influenced by the cold exhaust.

However, since the temperature measured on the rooftop might be affected by the cold exhaust to some extent, the value of ΔT obtained by this method tended to be underestimated. On the other hand, since the rooftop air temperature rises fastest after sunrise, the ΔT at each measurement point in this case becomes excessive. The sunrise time during each observation period was around 5:10 am for summer and 6:20 am for winter. Here, to avoid overestimation, we mainly discuss the evaluation value ΔT before 5:00 am. It should also be noted that as ΔT typically takes on a negative value, when evaluating the magnitude of its value, terms such as great, large or small indicate the magnitude of the absolute value.

3 Results and discussion

3.1 Spatial distribution of the cooling effect

Figure 8 shows the time series of the effect of cold exhaust on air temperatures (ΔT) at each measurement point of 1.5 m height, for each observation period. The temperature decline was indicated around 4:00–6:30 am for summer and 1:30–6:30 am for winter, which coincides with the operation time of the ASHPWHs. It can also be confirmed that the temperature decline is greatest on the northern side of the site with the largest number of cold exhaust emission sources. At each of the three measurement points on the northern side, the value of ΔT is larger than those at all the other points in other directions. In the summer, among the three points on the northern side, the western point N-1 shows the largest ΔT of −0.36 °C at 4:30 am; in the winter, the eastern point N-3 shows the largest ΔT of −0.40 °C at 3:50 am. Referring to the average operation status of each ASHPWH unit (Fig. 4), a rough relationship can be observed between the horizontal distribution of the number of operating units and ΔT on the northern side. At the summer peak time (4:30 am), the average number of units operating in the western columns (#1 and # 2) was 2.5, which is 1.25 times larger than the number (2.0) in the eastern columns (#3 and #4). At the winter peak time (3:50 am), the average number of units operating in the eastern columns was 5.0, which is 1.32 times larger than the number (3.8) in the eastern columns. Therefore, larger ΔT values are observed at the measurement points with a larger number of operating units in the vicinity.

However, ΔT is affected by the amount of exhaust, the linear distance between the emission source and the measurement point, and by complex factors, such as local airflow caused by obstacles (e.g., buildings, fences, and plants). Quantitatively examining these factors in detail is highly site-specific and beyond the scope of this study. The following discussion focuses on the northern side of the site; the average of ΔT at the N-1, N-2, and N-3 measurement points and the effective amount of exhaust heat H_e were used to perform a qualitative analysis to identify the meteorological factors affecting ΔT. The peak value of the average ΔT [°C] on the northern side of the building is −0.32, for summer (at 4:30 am) and winter (at 3:40 am). The effective amounts of cold exhaust H_e [kW] at each peak time are −11.4 and −14.8 in summer and winter, respectively (Fig. 5); thus, the sensitivities of temperature to cold exhaust ($\Delta T/H_e$) [°C/kW] are 0.028 and 0.022, respectively. The differing $\Delta T/H_e$ values for each season could be due to the difference in the atmospheric conditions during each observation period.

Figure 9a shows the time series of the average ΔT measured at the northern points (N-1, N-2, and N-3) and averaged for each wind direction and season. The ΔT [°C] values at peak times are −0.71 (at 5:00 am), −0.24 (at 4:40 am), and −0.32 (at 3:40 am) for days with southerly wind and summer and winter days with northerly wind, respectively. The cooling effect was significantly larger when the southern winds were dominant in the summer, and the thermal environment worsened, perhaps because southerly wind speeds tend to be low; thus, the diffusion of the cold exhaust is more difficult, and the exhaust tends to stay near the ground at the site.

Figure 9b shows the time series of the sensitivity of temperature to cold exhaust ($\Delta T/H_e$). At each peak time of ΔT, the values of $\Delta T/H_e$ [°C/kW] are 0.055 (at 5:00 am), 0.019 (at 4:40 am), and 0.022 (at 3:40 am) for days with southerly wind and summer and winter days with northerly wind, respectively. The value of $\Delta T/H_e$ is significantly larger for southerly wind days in the summer when the average wind speed is small (Table 1), indicating dependence on wind direction and wind speed. For northerly wind days, the value of $\Delta T/H_e$ is slightly greater in winter, despite a slightly greater wind speed, suggesting that dependence on other factors, such as the convective stability near the ground surface. The value of $\Delta T/H_e$ tends to be large immediately after the units start operating (and H_e is still small) and gradually decreases as H_e increases (Fig. 5). Therefore, ΔT peaks before H_e. This is because, as the

temperature near the ground decreases, the density difference between the cold exhaust and the air temperature decreases, making it harder for the cold exhaust to sink downward and to increase its advection diffusion to the surroundings. Focusing on the limited space within the site reveals that, as H_e input increases, the ratio of H_e going out by advection diffusion also increases, decreasing the sensitivity of temperature to cold exhaust $\Delta T/H_e$. Thus, a value of H_e must exist that can achieve the desired ΔT with maximum efficiency, suggesting that the cooling effect can be sustained for a longer time by adjusting H_e by controlling the number of operating units.

During the entire period of observation, August 20, 2008 marked the largest ΔT observed at 5:00 am, with calm wind (wind speed < 0.4 m/s) and air temperature T_a measured at the rooftop of 25.2 °C. Near the peak time, all measurement points 1.5-m above ground level on the northern side of the building registered ΔT of more than −1 °C; and all other measurement points at a 1.5-m height showed ΔT values of −0.4 °C to −0.6 °C (Fig. 10a). At 5:00 am, five of the 12 ASHPWH units on the northern side of the building (G-1, M-2, G-2, M3, and T-4) were in operation (Fig. 10b). The observed horizontal distribution of ΔT was roughly reproduced using a CFD simulation (see Appendix B). Figure 10 shows that the magnitude of ΔT at each measurement point is not simply determined by the number of operating units in the vicinity. For example, at 5:40 am, the number of units in operation reaches 8; however, the ΔT values observed at the three northern points range from −0.8 °C to −0.7 °C—approximately 74% of the value at 5:00 am. Immediately after that, two units stopped, and at 5:50 am, three units were in operation in the western columns (#1 and #2) and the eastern columns (#3 and #4); however, a significant ΔT of over −1.2 °C was observed only at the eastern point (N-3). These irregularities are attributable to more complex local airflows that cannot be captured by the measurements in this study.

Figure 11 shows the vertical profile of the ΔT as of 5:00 am in the summer, determined for each wind direction from the average value for each height at each temperature measurement point along the north-side wall of the building. On the southerly wind days, ΔT is extremely large near the ground, but that influence decreases rapidly with height, leaving little observable ΔT at a height of 8.2 m. On the other hand, during days with northerly winds, the ΔT near the ground is relatively small, but the rate of decline with height is also small, showing a more substantial ΔT at 8.2 m height than on southerly wind days. This vertical structure shows that, in the case of weaker southerly winds, cold exhaust is hardly diffused (partly because it is sheltered from the winds by the building), effectively cooling the air near the ground. However, when relatively strong northerly winds blow, cold exhaust is diffused upward along the north-side wall of the building, therefore the cooling effect near the ground is reduced.

3.2 Dependence of the cooling effect on local atmospheric conditions

Since the cold exhaust is heavier than the ambient air, it naturally sinks downward, and then spreads outward along the ground surface driven by its own weight. Its diffusion speed is likely affected by the local atmospheric conditions. Wind speed is one of the major factors that influence the horizontal advection of the cold. Wind direction is another influencing factor that defines the positional relationship between the building and emission source of the cold. In addition, the near-surface thermal convection is thought to affect the vertical diffusion of the cold.

Figure 12 shows the relationship between the sensitivity of the 1.5-m temperature to cold exhaust ($\Delta T/H_e$) and wind speed (1-h average prior to peak ΔT). ΔT is the average of the observed values at the N-1, N-2, and N-3 measurement points. The figure clearly demonstrates that the weaker the wind is, the greater the $\Delta T/H_e$ becomes. Considering that the UHI tends to be more intense on calm days, this could be advantageous from the perspective of improving the thermal environment. If we focus on the

northerly wind days, the locations of the summer and winter clusters overlap for the most part, and seasonal differences are hardly observed in the range of $\Delta T/H_e$. On the other hand, the cluster of southerly wind during the summer is found at a location away from the other two clusters indicating a higher sensitivity. This is likely due to the influence of the positional relationship between the building and the emission sources of the cold in addition to the wind speed. That is to say, when the exhaust outlets are placed on the leeward side of the building the wind has less effect on the diffusion of the cold because the building acts as a shelter from the wind. In this case, since the location of the outlets is mainly on the northern side of the building, we can expect the $\Delta T/H_e$ to become greater under southerly winds.

As an indicator for convective stability near the ground, we used the difference between the air temperature and ground surface temperature ($T_g - T_a$). Figure 13 shows, in the same manner as in Fig. 12, the relation between $\Delta T/H_e$ and $T_g - T_a$. The locations of summer and winter clusters hardly overlap in the range of $T_g - T_a$ clearly indicating that it was mostly unstable ($T_g > T_a$) or neutral ($T_g \approx T_a$) during the summer, while it was always stable ($T_g < T_a$) during the winter. In the range of $\Delta T/H_e$, the cluster of southerly wind is located above the other two clusters of northerly wind, as found in Fig. 12. On days with northerly winds, $\Delta T/H_e$ shows a slight tendency to increase as T_g drops below T_a, suggesting that the near-surface convective stability state slightly influences the diffusion of the cold exhaust at the building scale; however, this influence is small compared to that of the wind. This can be understood that since the cold exhaust near the building is much cooler (and heavier) than ambient air, the downward momentum of its gravity-driven flow is too large to be affected by the buoyancy forces from the weak thermal convection near the ground at night.

Figures 12 and 13 suggest that the wind (horizontal advection) has a substantial influence on the sensitivity $\Delta T/H_e$, while the influence from near-surface thermal convection is limited. To test the statistical significance of this result, we performed a multiple regression analysis with $\Delta T/H_e$ as a target variable and the three influencing factors (i.e., wind direction, wind speed and $T_g - T_a$) as explanatory variables. Here, wind direction is represented by a dummy variable that takes on the value 0 for south or 1 for north. The result (Table 2) confirmed that the most significant influencing factor is wind direction ($p<0.001$) followed by wind speed ($p=0.013$), and that $T_g - T_a$ has no significant influence ($p=0.062$). Here, a p value less than 0.05 was considered statistically significant.

4 Conclusions

Around a low-rise apartment building in which all apartments have air-source heat pump water heaters (ASHPWHs) installed, we observed the thermal environment in building scale during summer and winter. The following findings concerning the cooling effect of cold exhaust on ambient outdoor temperature are provided as:

(1) The greatest reduction in 1.5 m air temperature exceeded 1 °C and it was shown to be concentrated on the side where the exhaust outlets of ASHPWH were placed. A building-scale improvement in the outdoor thermal environment caused by the cold exhaust was clearly demonstrated.

(2) The outdoor cooling effect of the cold exhaust showed a tendency to increase when the exhaust outlets were placed on the leeward side of the building.

(3) The cooling effect also showed a tendency to increase when winds were weak. Since it was observed that the UHI becomes more intense on calm days, it is an advantage from the viewpoint of UHI alleviation.

(4) The thermal convective stability near the ground surface showed no significant influence over the

cooling effect.

As calm days with weak wind were minimal during the entire measurement period of this study, and no southerly wind days were observed during the winter, the study would benefit from further accumulation of data through additional observation cases. In this study, the temperature measurement points were limited within the site of the target building. To estimate the cooling effect of the cold exhaust beyond the boundary of the site, a city-block scale observation is required. It is possible that the convective stability state near the ground surface has some influence over the cooling effect in city-block (or wider) scale.

Although this study focused on direct impact on the outdoor thermal environment induced by ASHPWHs, its indirect impact on the annual energy consumption is also an interesting research topic. The reduction in outdoor temperature would reduce the cooling load in summer and increase the space heating load in winter. This is the case even though the reduced/increased demand in summer and winter, respectively, would be limited compared to the major contribution from significantly reduced energy consumption for water heating. Since data on energy demand were not available in this study, assessing the impact on annual energy demand is a topic for future research.

Through this study, it was indicated that an area-wide installation of ASHPWHs has the potential to improve the deteriorated nighttime thermal environment by recovering excess urban heat. In megacities of developing countries located in tropical regions, further degradation of the urban thermal environment will occur as a result of global warming and UHI, and energy demand for air conditioning and hot water is expected to increase rapidly. These megacities are promising candidates where the outdoor cooling effect of ASHPWHs will be most effective and beneficial. In the tropics, neither poor performance from low temperatures is likely to occur nor is there an impact on space heating energy due to the outdoor cooling effect.

The findings from this study give a new perspective for urban planning and architectural design for residential areas. For example, locations of residential buildings and outdoor units of ASHPWHs can be planned with consideration for the main wind direction of summer night to maximize the cooling effect of the cold exhaust. If the priority is given to human health, ASHPWHs can be programmed to operate during earlier (and hotter) nighttime. The urban-scale strategic use of the cold energy produced by heat pumps should be considered as a potential method of both mitigating and adapting to climate change.

Appendix A. Measurement of exhaust air from outdoor unit

This observational study had many limitations, as it was conducted on a real house, and directly measuring the power consumption of each ASHPWH unit or the temperature and airflow of the exhaust was not possible. Therefore, the temperature and air velocity of the cold exhaust from the units were measured separately to verify the energy of the cold exhaust.

The measurements were performed on March 12, 2009, when the wind was weak, at an experimental house located in Yokohama City, Kanagawa Prefecture. The ASHPWH unit used for the measurements was of the same type (Corona, CHP-452) as the ones used in this study. The outdoor unit was installed on the ground beside the house, and the center of the air outlet was located at approximately 0.5 m above the ground.

Thermistor thermometers (T&D, RTR-52) fitted with solar shields were used to measure the ambient temperature, intake, and exhaust air. To capture the temperature distribution of the exhaust within the blowing area at the air outlet, four measurement points were set on the upper, lower, left,

and right sides of the area (U, D, L, and R in Fig. 14). Intake air temperatures (T_{in}) were measured at two points near the inlet of the outdoor unit, and the averaged values were used for the analysis. The ambient air temperatures were measured at 1.5 m above the ground and approximately 5 m horizontally from the outdoor unit side. The data measurement interval for the thermistor thermometer was set to 15 s, and the average value of over 1 min was used to analyze the results.

A rotating vane anemometer (TSI, Model 5725) was used to measure the air velocity of the exhaust air. Using the same method as for air temperature, the air velocity was measured at four points in the vertical and horizontal directions from the center of the air outlet (Fig. 14). The measurement interval and time constant (averaging period) were set to 1 and 10 s, respectively, and the reading was taken when the fluctuation of the displayed value had settled.

Figure 15 shows the air temperature measurements taken from 9:15 am to 13:40. The ASHPWH unit started at 9:23 am and stopped at 13:28. The intake air temperature remains approximately 0.8 °C lower than the ambient temperature during the morning but rises approximately 6.4 °C with the ambient temperature throughout the operating time of the unit, with no notable effect from the cold exhaust. The exhaust temperature readings at all four points decrease significantly as soon as the unit starts. Thereafter, they rise in sync with the ambient air temperature and quickly return to the same level as the ambient air temperature when the unit stops. Throughout the operating time of the unit, the deviations from the intake air temperature remained nearly constant. During the morning, the values at U and R were approximately 0.5 °C higher than the values at D and L, indicating slight temperature irregularities within the blowing area of the air outlet. However, because the values at U and R and those at D and L are in good agreement, the four-point average is regarded as the average temperature of the entire exhaust. By averaging the temperature deviation from the intake air temperature throughout the unit operation time (9:16 am−13:40), a four-point average of −6.75 °C was obtained.

The air velocity of the exhaust air was measured separately from the air temperature. The values of air velocity [m/s] obtained at measuring points U, D, L, and R were 3.4, 3.3, 3.3, and 3.1, respectively. Here, the four-point average of 3.26 m/s is considered the average velocity of the exhaust air immediately after leaving the vent.

The amount of energy of the cold exhaust from an ASHPWH unit H_1 [kW] can be expressed as:

$$H_1 = E - Q, \tag{3}$$

where E and Q represent the electricity consumption [kW] and heating capacity [kW] of the ASHPWH, respectively. According to the rated values specified by the manufacturer, Q is a constant value of 4.5, and E depends on the outdoor temperature, humidity, supply water temperature, and hot water temperature (Table 3). Because the data available for this study are limited, only the outdoor dry-bulb temperature is considered, assuming that the hot water temperature was set at 65 °C. The electric consumption E can be approximated by a linear equation of the air temperature T_a [K] (R^2>0.999) as follows:

$$E = -0.0128T_a + 4.83. \tag{4}$$

In the measurement, the average intake air temperature T_a during the operation of the ASHPWH unit was 285.16 K (12 °C). Therefore, the average value of H_1 can be estimated at −3.32 kW from Eqs. 3 and 4.

Using the measured air temperature values of the exhaust T_{ex} [K] and its air velocity V [m/s], H_1 [kW] can be expressed as:

$$H_1 = \rho C_p (T_{ex} - T_a) VA/1000 \quad (5)$$

$$\rho = P/(RT_a), \quad (6)$$

where ρ, C_p, A, P, and R are the density of air [kg/m^3], constant pressure heat capacity of air (1004 J/kg/K), effective blowing area of the air outlet [m^2], atmospheric pressure (101300 Pa), and gas constant of dry air (287 J/kg/K), respectively. The air velocity is generally not constant within the blowing area, as it is smaller near the outer edge and the rotation axis of the fan; thus, the effective blowing area is assumed to be smaller than the actual size of the vent aperture. Here, we assume that A is 0.121 m^2, which corresponds to the area of the region between the concentric circles with diameters of 436 and 189 mm, which is approximately 85% of the size of the air outlet aperture (Fig. 14). Furthermore, using $T_{ex} - T_a$ (−6.75 K), T_a (285.16 K), and V (3.26 m/s) obtained from the measurements, H_1 was calculated from Eqs. 5 and 6, yielding a value of −3.31 kW. The value obtained here is in good agreement with the value of H_1 (−3.32 kW) calculated from Eqs. 3 and 4. Therefore, based on the measured values of temperature and air velocity, the amount of energy of the cold exhaust roughly corresponds to the estimated values of the heating capacity and electric consumption specified by the manufacturer.

Appendix B. Computational fluid dynamics (CFD) simulation

In this study, the number of temperature measurement points were too small to produce high-resolution 3-dimensional images of air temperature distribution around the building. The spatially dispersed distribution of emission sources makes the evaluation of temperature sensitivity to cold exhaust even more difficult. The location of the measurement points was limited to the site of the target building; hence, estimating the cooling effect of the cold exhaust beyond the boundary of the site was not possible. In this appendix, a computational fluid dynamics (CFD) simulation was performed to reproduce the results of the observation. This simulation study has the following three primary objectives: (1) visualizing a 3-dimensional distribution of air temperature around the building to better understand the behavior of the cold exhaust emitted from the outlets; (2) evaluating the relative effect of the vertical and horizontal locations of the exhaust outlets on the temperature at specified measurement points; and (3) understanding the impact of the cold exhaust beyond the boundary of the site.

We attempted to reproduce the observed results from August 20, 2008 at 5:00 am (Fig. 10) with a three-dimensional simulation using a standard k–ε turbulence flow model (AKL FlowDesigner 2020). The analysis area was 314 m east-west × 375 m north-south × 25 m vertical, with 4.0 million mesh elements (200 × 200 × 100). The target building, site boundary, and outdoor units of the ASHPWH were set as shown in Fig. 2. Two 2-m-high fences with 0% opening ratio were placed on the north and south boundaries of the site; those with 90% opening ratio were on the east and west boundaries. Surrounding buildings were selected after considering their influence on the airflow. The inflow boundary conditions included a southerly wind at 1/4 low power with a speed of 0.1 m/s at an altitude of 11.5 m and temperature of 25.2 °C. The temperature of the cold exhaust at the outlet was set to 17.8 °C, and the airflow rate was 1,423.7 m^3/h per unit (air velocity: 3.26 m/s, blowing area: 0.121 m^2), which was estimated based on measured values from a real machine (Appendix A). Steady-state calculations were performed with a convergence criterion of less than 0.1% residual, and non-steady-state calculations were performed with a time interval of 30 s.

Figure 16 depicts the simulated vertical cross section of the air temperature distribution next to the cold exhaust outlets on the northern side of the building, with the three ASHPWH units in column #1 operating concurrently. The temperature distribution shows that the cold exhaust sinks and remains

near the ground. Much of the cold exhaust emitted from higher altitudes extends directly beyond the site boundary. Therefore, higher exhaust outlets are assumed to exert a smaller temperature effect at the measurement points within the boundary. Similarly, the low interference of the mesh fences on the east and west boundaries on outgoing airflow lead to different temperature effects between the cold exhaust from the outer (#1 and #4) and inner (#2 and #3) columns.

To compare the effect of the location of the exhaust outlets, five case simulations (Table 4) were performed by steady-state calculations. Cases T, M, and G are scenarios comparing the effect of exhaust height, with four units operating on the top, middle, and ground floors. Likewise, cases I and O are scenarios comparing the effect of the horizontal position, with six units operating in the inner (#2 and # 3) and outer (#1 and #4) columns. For each case, the simulated horizontal distribution of the 1.5-m air temperature at the northern side of the site is shown in Fig. 17. As temperature reference points, the values are indicated at positions corresponding to the N-1, N-2, and N-3 measurement points. For cases T, M, and G, the average values of deviation from the inflow temperature (25.2 °C) are −0.83, −1.13, and −2.57 °C, respectively. For cases I and O, the average deviation values are −1.50 and −1.37 °C, respectively. The results show that under calm conditions, the cold exhaust from the middle and top floors registered 44% and 32% of the temperature effect of the ground floor, respectively; further, the cold exhaust from the outer two columns registered 91% of the temperature effect of the inner two columns. The values obtained were used as the weighting factors in Eq. 2 for the effective amount of cold exhaust H_e.

The reproduction simulation was performed for the period from 4:00–5:00 am on August 20, 2008, using non-steady state calculations. In the simulation, the ASHPWH units on the northern side were set in operation in accordance with the monitored state in the observation (Fig. 10b); that is, the units are all off at 4:00 am and initiate sequentially; thus, at 5:00 am, five units (G-1, M-2, G-2, M-3, and T-4) are in operation. Of the four units on the southern side that were not monitored in the observation, two (one on the top floor in the western column #5 and one on the middle floor in the eastern column #6) were assumed to be in operation from 4:00–5:00 am.

The simulation results at 5:00 am are shown in Fig. 18. The areas around the building show a decrease in temperature, with changes of approximately −1 and −0.5 °C on the northern side and the other three sides, respectively (Fig. 18a). The situation reproduced in the model roughly matches the results of the actual observations at 5:00 am (Fig. 10). A more detailed examination reveals that the temperature effects at positions corresponding to the N-1, N-2, and N-3 measurement points are −2.4, −1.4, and −1 °C, respectively, with a large gradient in the east-west direction. This can be explained by the fact that the units on the ground floor, which have the largest temperature effect, operate only in the eastern two columns. However, this simulation result is not consistent with the observed results, where all measured values are almost uniformly within the range of −1.1 to −1.0 °C. This discrepancy between the simulation and the observation suggests the influence of more complex local airflows that cannot be captured by the measurements in this study.

Outside the site, the cooled region (where 1.5-m air temperatures were 0.5−1.5 °C lower than the inflow air) extends beyond the site boundary to the surrounding areas, forming a cool spot the size of a city block. Much of the cold exhaust from the ground floor, in particular, flows into the north-south street on the west side of the target building, where the 1 and 0.5 °C-cooled regions reach approximately 20 and 40 m downstream, respectively (Fig. 18b). The cold air accumulates in the space between the target building and another building located approximately 10 m to the north, and the altitude of the 1° C-cooled region reaches more than 4 m above the ground (Fig. 18c).

Acknowledgement We greatly thank the anonymous reviewers for their constructive suggestions and

insightful comments.

Author contribution K. Yamaguchi: conceptualization, methodology, validation, formal analysis, investigation, resources, data curation, writing - original draft, visualization; T. Ihara and Y. Kikegawa: methodology, investigation, resources

Ethics approval Not applicable

Consent to participate Not applicable

Consent for publication Not applicable

Reference

Adelia AS, Yuan C, Liu L (2019) Shan RQ, Effects of urban morphology on anthropogenic heat dispersion in tropical high-density residential areas. Energy & Buildings 186: 368–383. https://doi.org/10.1016/j.enbuild.2019.01.026

Agency for Natural Resources and Energy (ANRE) (2019) Energy White Paper 2019 (In Japanese)

Atwater MA (1972) Thermal effects of urbanization and industrialization in the boundary layer. Boundary-Layer Met. 3: 229–245. https://doi.org/10.1007/BF02033921

Bureau of Social Welfare and Public Health, Tokyo Metropolitan Government (2019) Situation of Heat Stroke Deaths in summer of 2019 (Tokyo 23 wards). (in Japanese) https://www.fukushihoken.metro.tokyo.lg.jp/kansatsu/oshirase/R01-heatstroke.html

Cecchinato v, M. Corradi, E. Fornasieri, L. Zamboni (2005) Carbon dioxide as refrigerant for tap water heat pumps: a comparison with the traditional solution, Int. J. Refriger 28 (8): 1250–1258. https://doi.org/10.1016/j.ijrefrig.2005.05.019

Chen H, Ooka R, Huang H, Tsuchiya T (2009) Study on mitigation measures for outdoor thermal environment on present urban blocks in Tokyo using coupled simulation. Building and Environment 44: 2290–2299. https://doi.org/10.1016/j.buildenv.2009.03.012

Department for Business, Energy and Industrial Strategy (BEIS) (2019) Energy Consumption in the UK (ECUK) 2019. https://www.gov.uk/government/statistics/energy-consumption-in-the-uk

Ecotope and NEEA (2015) Heat Pump Water Heater Model Validation Study, Report #E15-306. https://ecotopewebstorage.s3.amazonaws.com/2015_001_1_HPWHModelVal.pdf

Energy Information Administration (EIA) (2018) 2015 Residential Energy Consumption Survey (RECS). https://www.eia.gov/consumption/residential/data/2015

Fan HL, Sailor DJ (2005) Modeling the impacts of anthropogenic heating on the urban climate of Philadelphia: a comparison of implementations in two PBL schemes. Atmos. Environ 39 (1): 73–84. http://dx.doi.org/10.1016/j.atmosenv.2004.09.031

Guo JJ, Wu JY, Wang RZ, Li S 82011) Experimental research and operation optimization of an air-source heat pump water heater. Applied Energy 88: 4128–4138. https://doi.org/10.1016/j.apenergy.2011.04.012

Ichinose T, Shimodozono K, Hanaki K (1999) Impact of anthropogenic heat on urban climate in Tokyo. Atmos. Environ 33 (24–25): 3897–3909. https://doi.org/10.1016/S1352-2310(99)00132-6

IEA (2018) The Future of Cooling, IEA, Paris. https://www.iea.org/reports/the-future-of-cooling

Ihara T, Takane Y, Genchi Y (2015) Estimation of DALY loss due to heat stroke and sleep disturbance caused by air temperature rise in Tokyo, Japan. The 9th International Conference on Urban Climate (ICUC-9), Centre de Congrès Pierre Baudis (Toulouse, France), 20-24 Jul 2015

IPCC AR4 WG2 (2007) Parry ML, Canziani OF, Palutikof JP, van der Linden PJ, Hanson CE (ed.), Climate Change 2007: Impacts, Adaptation and Vulnerability, Contribution of Working Group II to the Fourth Assessment Report of the Intergovernmental Panel on Climate Change, Cambridge University Press, ISBN 978-0-521-88010-7 (pb: 978-0-521-70597-4)

Johnson EP (2011) Air-source heat pump carbon footprints: HFC impacts and comparison to other heat sources, Energy Policy 39 (3): 1369–1381. https://doi.org/10.1016/j.enpol.2010.12.009

Karkour S, Ihara T, Kuwayama T, Yamaguchi K, Itsubo N (2021) Life Cycle Assessment of Residential Air Conditioners Considering the Benefits of Their Use: A Case Study in Indonesia. Energies 14(2):447. https://doi.org/10.3390/en14020447

Kim D, Myeong S, Cha D, Kim Y (1019) Novel optimized operating strategies of two-phase injection heat pumps for achieving best performance with safe compression. Energy 187: 115925. https://doi.org/10.1016/j.energy.2019.115925

Kimura F, Takahashi S (1991) The effects of land-use and anthropogenic heating on the surface temperature in the Tokyo Metropolitan area: a numerical experiment, Atmos. Environ. Part B Urban Atmos. 25 (2): 155–164. https://doi.org/10.1016/0957-1272(91)90050-O

Kusaka H, Kimura F (2004) Thermal effects of urban canyon structure on the nocturnal heat island: numerical experiment using a Mesoscale model coupled with an urban canopy model. J. Appl. Meteorology 43 (12): 1899–1910. http://dx.doi.org/10.1175/jam2169.1

Morrison GL, Anderson T, Behnia M. (2004) Seasonal performance rating of heat pump water heaters. Solar Energy 76:147–52. https://doi.org/10.1016/j.solener.2003.08.007

Nastos PT, Matzarakis A. (2008) Human-Biometeorological Effects on Sleep Disturbances in Athens, Greece: A Preliminary Evaluation. Indoor and Built Environment 17(6):535-542. https://doi.org/10.1177/1420326X08097706

Nekså P, Rekstad H, Zakeri GR, Schiefloe PA (1998) CO_2-heat pump water heater: characteristics, system design and experimental results, Int. J.Refriger 21 (3): 172–179. https://doi.org/10.1016/S0140-7007(98)00017-6

Ng E, Chen L, Wang Y, Yuan C (2012) A study on the cooling effects of greening in a high-density city: an experience from Hong Kong. Building and Environment 47, 256–271. https://doi.org/10.1016/j.buildenv.2011.07.014

Obradovich N, Migliorini R, Mednick SC, Fowler JH (2017) Nighttime temperature and human sleep loss in a changing climate. Sci Adv. 3(5):e1601555. https://doi.org/10.1126/sciadv.1601555

Ohashi Y, Genchi Y, Kondo H, Kikegawa Y, Yoshikado H, Hirano Y (2007) Influence of air-conditioning waste heat on air temperature in Tokyo during summer: numerical experiments using an urban canopy model coupled with a building energy model. J. Appl. Meteorol. Climatol. 46 (1): 66–81. http://dx.doi.org/10.1175/Jam2441.1

Rosenfeld, AH, Akbari H, Bretz S, Fishman BL, Kurn DM, Sailor D, Taha H (1995) Mitigation of urban heat islands: materials, utility programs, updates. Energy and Buildings 22, 255–265.

https://doi.org/10.1016/0378-7788(95)00927-P

Ryu Y-H, Baik JJ (2012) Quantitative Analysis of Factors Contributing to Urban Heat Island Intensity. J. Appl. Meteorol. Climatol. 51(5): 842–854. https://doi.org/10.1175/JAMC-D-11-098.1

Santamouris M (2012) Cooling the cities – A review of reflective and green roof mitigation technologies to fight heat island and improve comfort in urban environments. Solar Energy 103: 682–703. https://doi.org/10.1016/j.solener.2012.07.003

Savio P, Cynthia R Solecki WD, Slosberg RB (2006) Mitigating New York City's Heat Island with Urban Forestry, Living Roofs, and Light Surfaces. New York City Regional Heat Island Initiative. The New York State Energy Research and Development Authority, Albany, NY.

Shapiro C, Puttagunta S (2013) Field Performance of Heat Pump Water Heaters in The Northeast, NREL, Golden, CO. https://www.nrel.gov/docs/fy16osti/64904.pdf

Singh H, Muetze A, Eames PC (2010) Factors influencing the uptake of heat pump technology by the UK domestic sector, Renewable Energy 35: 873–878. https://doi.org/10.1016/j.renene.2009.10.001

Synnefa A, Dandou A, Santamouris M, Tombrou M (2008) On the use of cool materials as a heat island mitigation strategy. Journal of Applied Meteorology Climatology 47, 2846–2856. https://www.jstor.org/stable/26172775

Tello-Oquendo FM, Navarro-Peris E, Gonzálvez-Maciá J (2019) Comparison of the performance of a vapor-injection scroll compressor and a two-stage scroll compressor working with high pressure ratios. Applied Thermal Engineering 160: 114023. https://doi.org/10.1016/j.applthermaleng.2019.114023

van Loenhout JAF, le Grand A, Duijm F, Greven F, Vink NM, Hoek G, Zuurbier M (2016) The effect of high indoor temperatures on self-perceived health of elderly persons, Environmental Research 146: 27–34. https://doi.org/10.1016/j.envres.2015.12.012

Wei W, Ni L, Wang W, Yao Y (2020a) Experimental and theoretical investigation on defrosting characteristics of a multi-split air source heat pump with vapor injection. Energy and Buildings 217: 109938. https://doi.org/10.1016/j.enbuild.2020.109938

Wei W, Ni L, Zhou C, Wang W, Xu L, Yang Y, Yao Y (2020b) Technical, economic and environmental investigation on heating performance of quasi-two stage compression air source heat pump in severe cold region. Energy and Buildings 223: 110152. https://doi.org/10.1016/j.enbuild.2020.110152

Yokoyama R, Shimizu T, Ito K, Takemura K (2007) Influence of ambient temperatures on performance of a CO_2 heat pump water heating system. Energy 32: 388–98. https://doi.org/10.1016/j.energy.2006.06.020

Zhou Y, Shepherd JM (2010) Atlanta's urban heat island under extreme heat conditions and potential mitigation strategies. Natural Hazards 52, 639–668. http://dx.doi.org/10.1007/s11069-009-9406-z

Tables

Table 1 Overview of weather by wind direction during the operation times of ASHPWH. Wind directions are grouped into two main directions: north (from WNW to ENE) and south (from ESE to WSW)

Observation period	Main wind direction	Average wind speed	Average air temperature	Average ground surface temperature	Total # of observed days
Summer (4:00–6:30 am)	North	1.0 m/s	22.6 °C	23.5 °C	18
	South	0.4 m/s	25.4 °C	25.4 °C	4
Winter (1:30–6:30 am)	North	1.2 m/s	5.4 °C	3.7 °C	11
	South	–	–	–	0

Table 2 Result of multiple regression analysis among the influencing factors on the $\Delta T/H_e$ [°C/kW] shown in Figs. 12 and 13. Wind direction is represented by a dummy variable that takes on the value 0 for south or 1 for north

Explanatory variable	Partial regression coefficient	p-value
Intercept	6.8×10^{-2}	6.5×10^{-14}
Wind Direction	-3.4×10^{-2}	2.0×10^{-6}
Wind Speed [m/s]	-8.9×10^{-3}	1.3×10^{-2}
T_g-T_a [°C]	-2.2×10^{-3}	6.2×10^{-2}
R^2	0.73	($p < 0.001$)

Table 3 Heating capacity and electric consumption of the ASHPWH unit under conditions specified by the manufacturer

Outdoor dry-bulb temperature [°C]	25	16	7	7
Outdoor wet-bulb temperature [°C]	21	12	4	6
Supply water temperature [°C]	24	17	9	9
Hot water temperature [°C]	65	65	65	90
Heating capacity [kW]	4.5	4.5	4.5	4.5
Electricity consumption [kW]	1.02	1.14	1.25	1.54

Table 4 Setup for simulation cases

Cases	Units in operation
T	T-1, T-2, T-3, T-4
M	M-1, M-2, M-3, M-4
G	G-1, G-2, G-3, G-4
I	T-2, G-2, M-2, T-3, M-3, G-3
O	T-1, G-1, M-1, T-4, M-4, G-4

Figure Captions

Fig. 1 Conceptual diagram of the energy and heat balance of a hot water supply system: (a) gas/electric water heater and (b) heat pump water heater

Fig. 2 (a) Location of columns of outdoor ASHPWH units and air temperature measurement points 1.5-m above ground at the site (top view). The red triangles indicate the measurement points for ground surface temperatures. (b) Location of outdoor ASHPWH units and air temperature measurement points along the northern wall of the building (front view). The measurement points only were set during the summer observation period

Fig. 3 Thermistor thermometer installed in front of the exhaust outlet of the outdoor unit

Fig. 4 Average operating rate of each ASHPWH unit on the northern side of the building for each observation period: (a) summer and (b) winter. The vertical axis of each panel ranges from 0–100%. The time interval is 10 min

Fig. 5 Time series of estimated average total amount of cold exhaust H_n and effective amount of cold exhaust H_e (with standard deviation error bars) during each summer and winter observation period. Negative values indicate the amount of heat energy absorbed from outdoor air

Fig. 6 Observed air temperatures on the roof of the target building. For each observation period, the shaded area shows the full ranges of observed values with the thick line indicating average values

Fig. 7 Wind rose for the operation times of ASHPWH during each observation period: (a) summer (4:00–6:30 am) and (b) winter (1:30–6:30 am)

Fig. 8 Average effect of cold exhaust on average 1.5-m air temperatures (ΔT) at each measurement point for each observation period: (a) summer and (b) winter

Fig. 9 (a) Average of the effect of cold exhaust on air temperatures (ΔT) at three measurement points (N-1, N-2, and N-3) on the northern side of the site (sorted by observation period and wind direction). (b) The sensitivity of temperature to cold exhaust ($\Delta T/H_e$)

Fig. 10 (a) Effect of cold exhaust on air temperatures (ΔT) observed at each measurement point of 1.5-m height; (b) operation status of each ASHPWH unit on the northern side of the building, on August 20, 2008

Fig. 11 Vertical profile of the average effects of cold exhaust on temperature (ΔT) along the north side of the building at 5:00 am in the summer observation period (sorted by main wind direction)

Fig. 12 Relationship between the sensitivity of 1.5-m temperature to cold exhaust ($\Delta T/H_e$) and wind speed. The value of ΔT is the average of those observed at points N-1, N-2, and N-3. The values of $\Delta T/H_e$ are a 10-min average taken at the peak time of ΔT for each day; the wind speed values are 1-h averages prior to the peak time. The straight line is a linear regression of data on days with northerly wind

Fig. 13 Same as Fig. 12, but for the difference between the air temperature and ground surface temperature ($T_g - T_a$; 1-hour average before peak time of ΔT) instead of the wind speed

Fig. 14 Measurement points of temperature and air velocity at the air outlet of the outdoor unit. The red shaded area indicates the estimated effective blowing area of the outlet

Fig. 15 Time series of the temperature of the ambient air, the intake, and the exhaust of the outdoor unit. The exhaust temperatures are measured at points U, L, R, and D (indicated in Fig. 14)

Fig. 16 Simulated vertical cross section of air temperature distribution along cold exhaust outlets

Fig. 17 Simulated horizontal distribution of 1.5-m air temperature on the northern side of the site for cases (a) T, (b) M (c) G, (d) I, and (e) O. The red circles indicate the N-1, N-2, and N-3 measurement points

Fig. 18 Simulated distribution of air temperature at 5:00 am on August 20, 2008: (a) horizontal distribution 1.5 m above the ground, (b) vertical cross section along north-south line BB', and (c) same as (b), but for line CC'

Figures

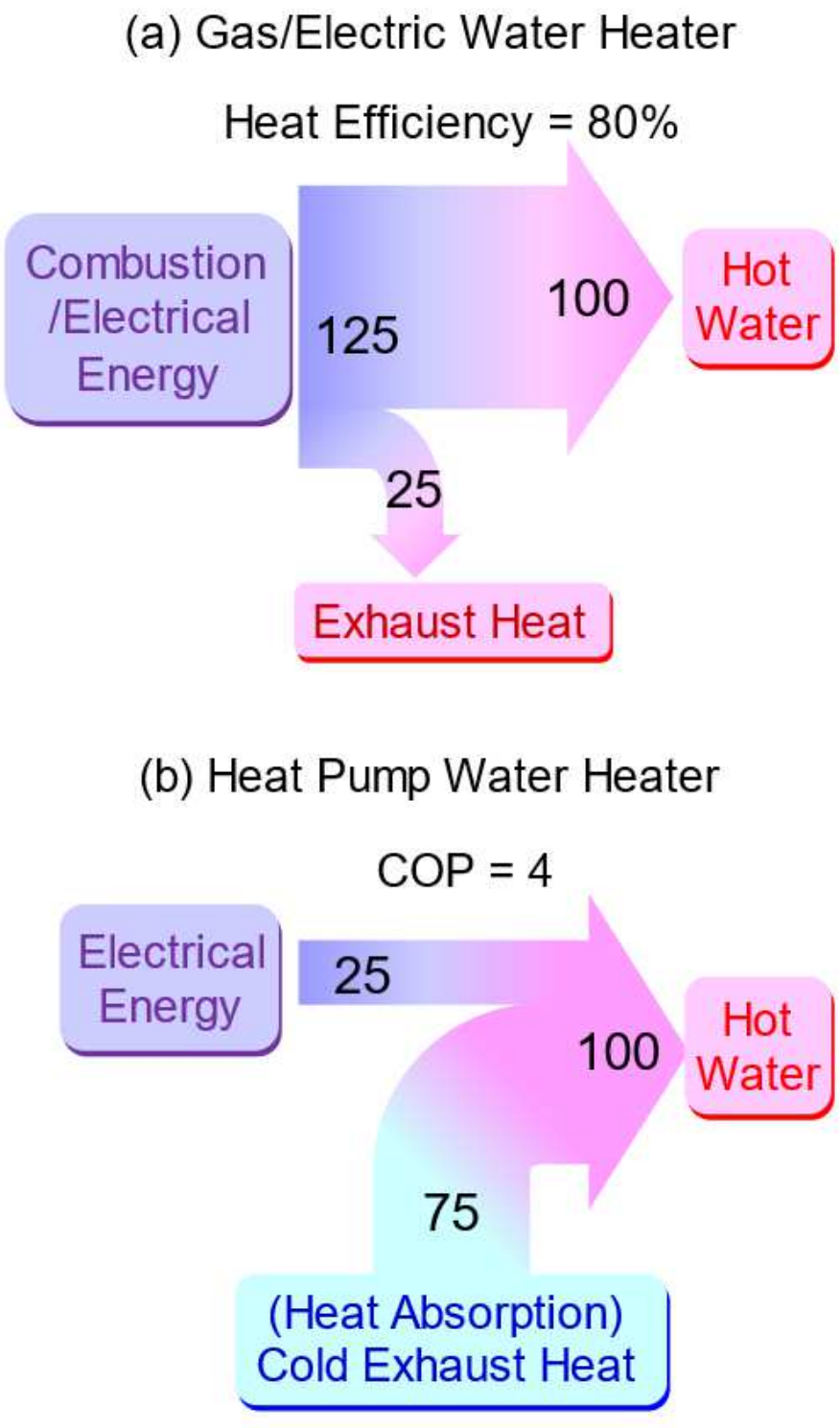

Figure 1

Conceptual diagram of the energy and heat balance of a hot water supply system: (a) gas/electric water heater and (b) heat pump water heater

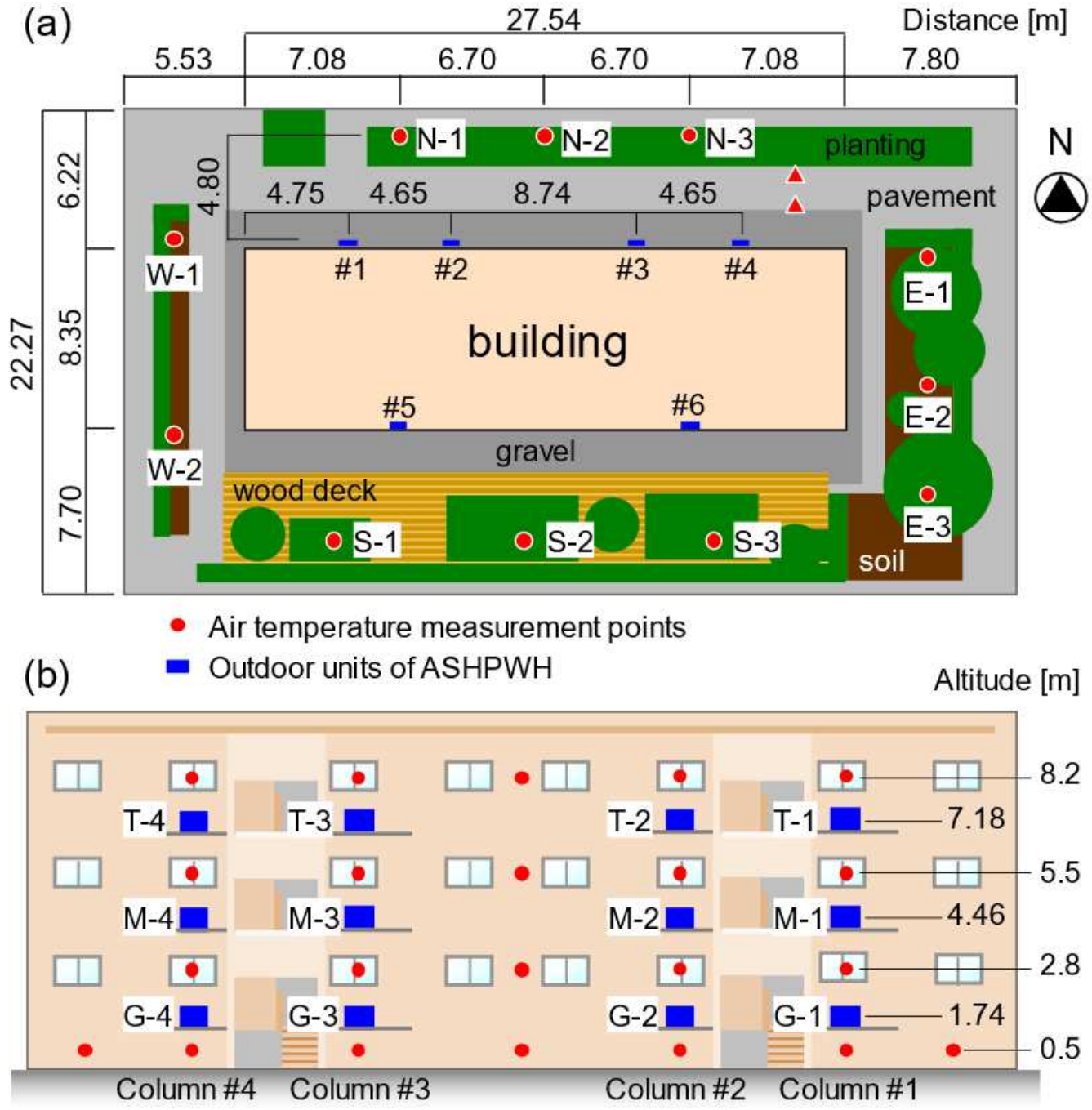

Figure 2

(a) Location of columns of outdoor ASHPWH units and air temperature measurement points 1.5-m above ground at the site (top view). The red triangles indicate the measurement points for ground surface temperatures. (b) Location of outdoor ASHPWH units and air temperature measurement points along the northern wall of the building (front view). The measurement points only were set during the summer observation period

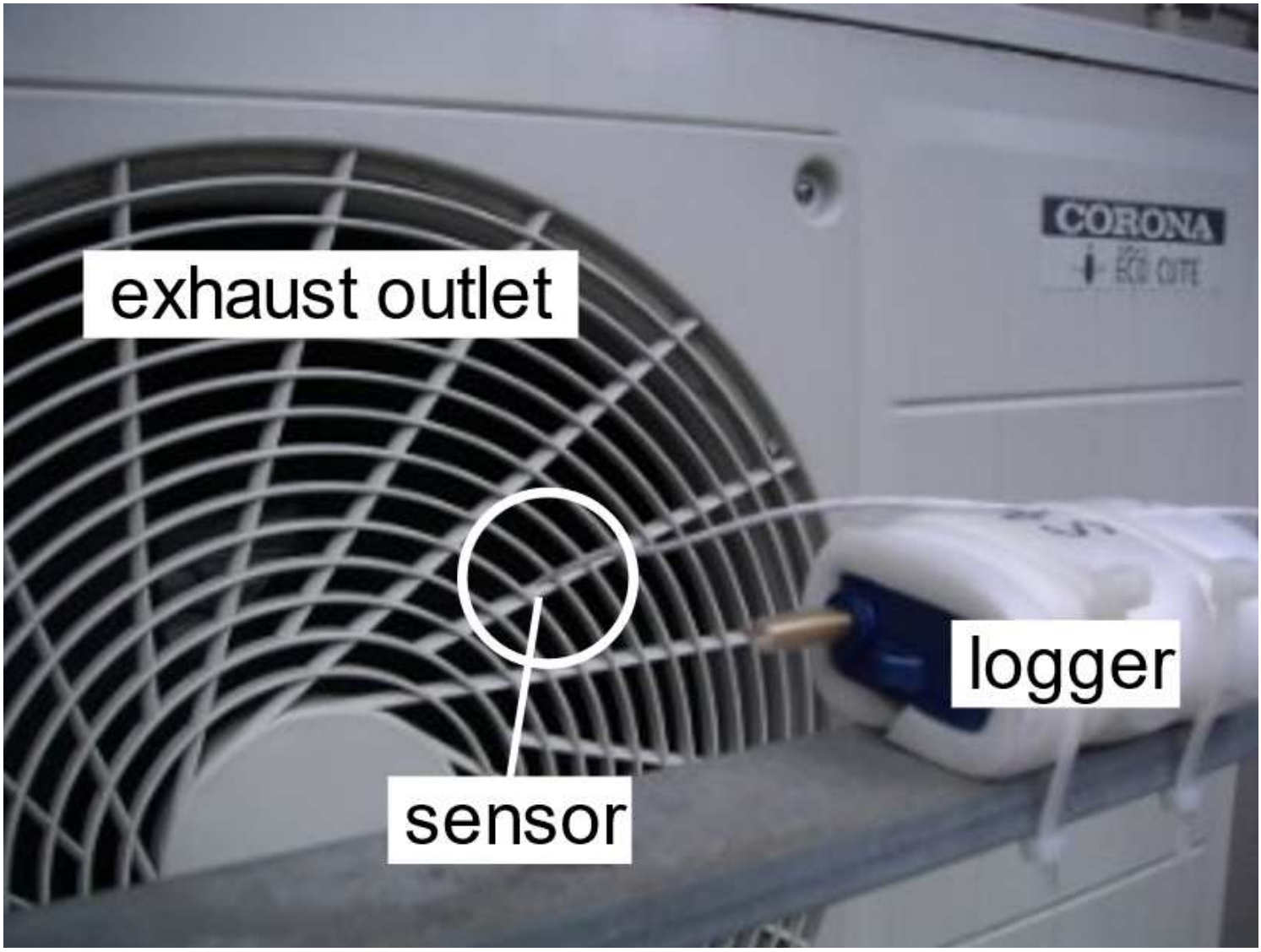

Figure 3

Thermistor thermometer installed in front of the exhaust outlet of the outdoor unit

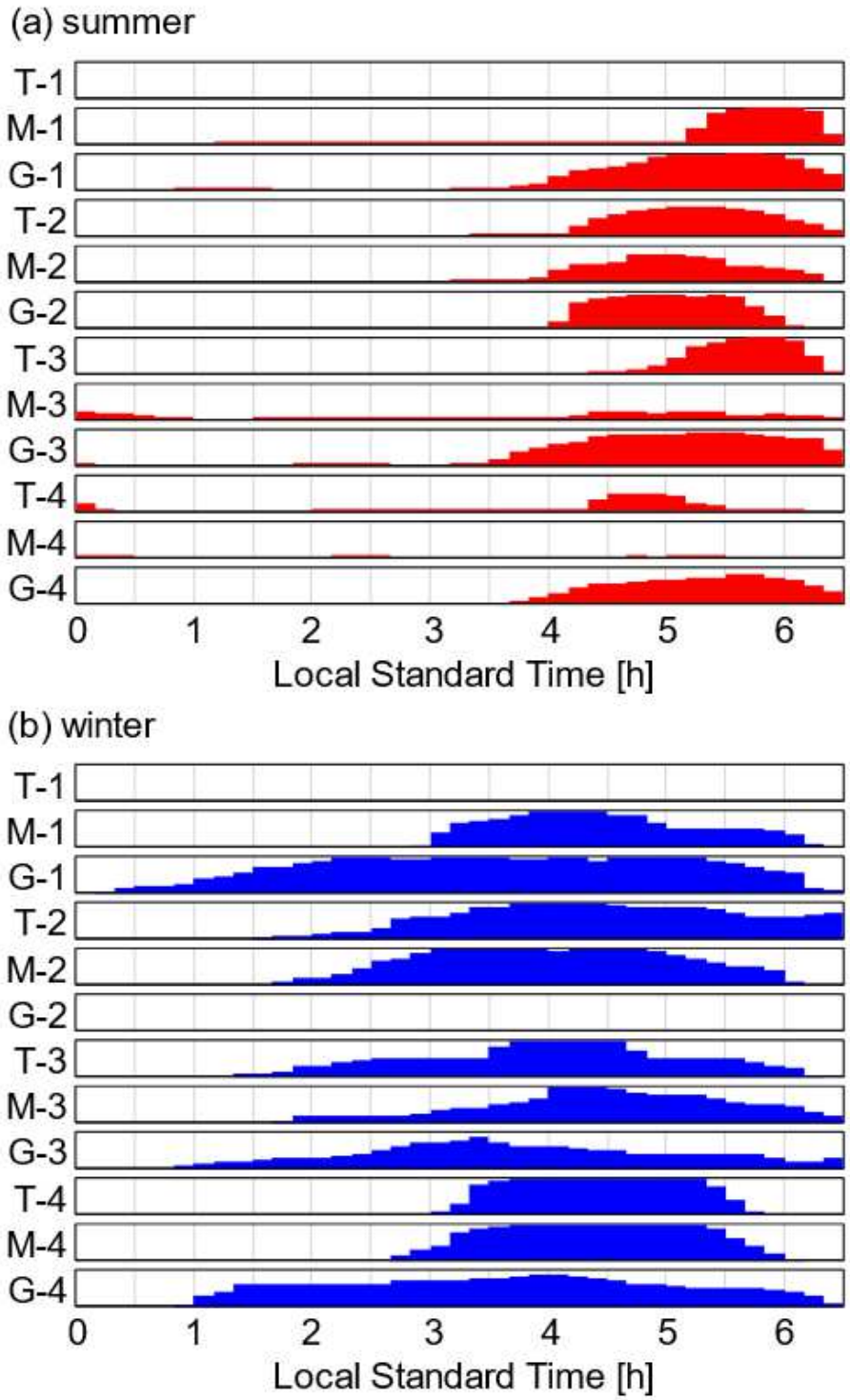

Figure 4

Average operating rate of each ASHPWH unit on the northern side of the building for each observation period: (a) summer and (b) winter. The vertical axis of each panel ranges from 0–100%. The time interval is 10 min

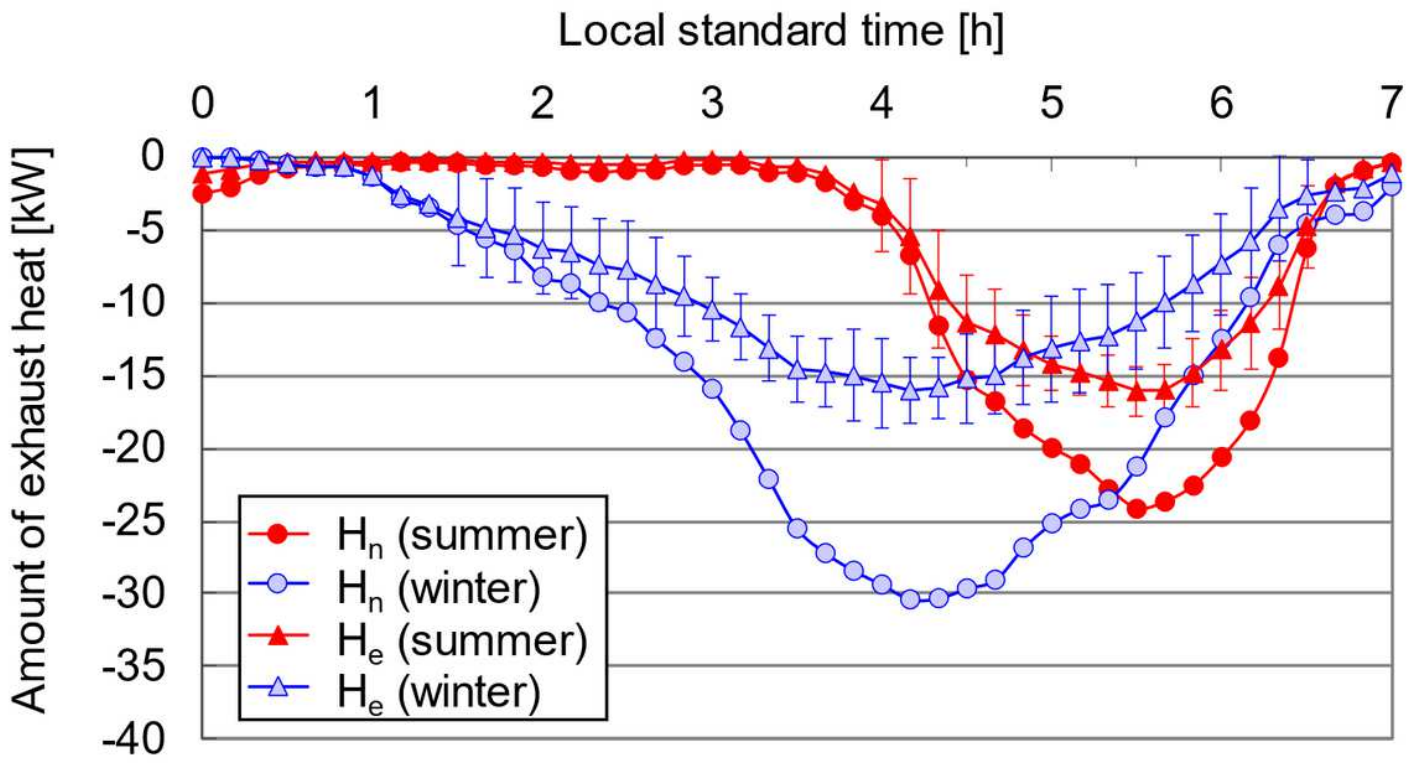

Figure 5

Time series of estimated average total amount of cold exhaust Hn and effective amount of cold exhaust He (with standard deviation error bars) during each summer and winter observation period. Negative values indicate the amount of heat energy absorbed from outdoor air

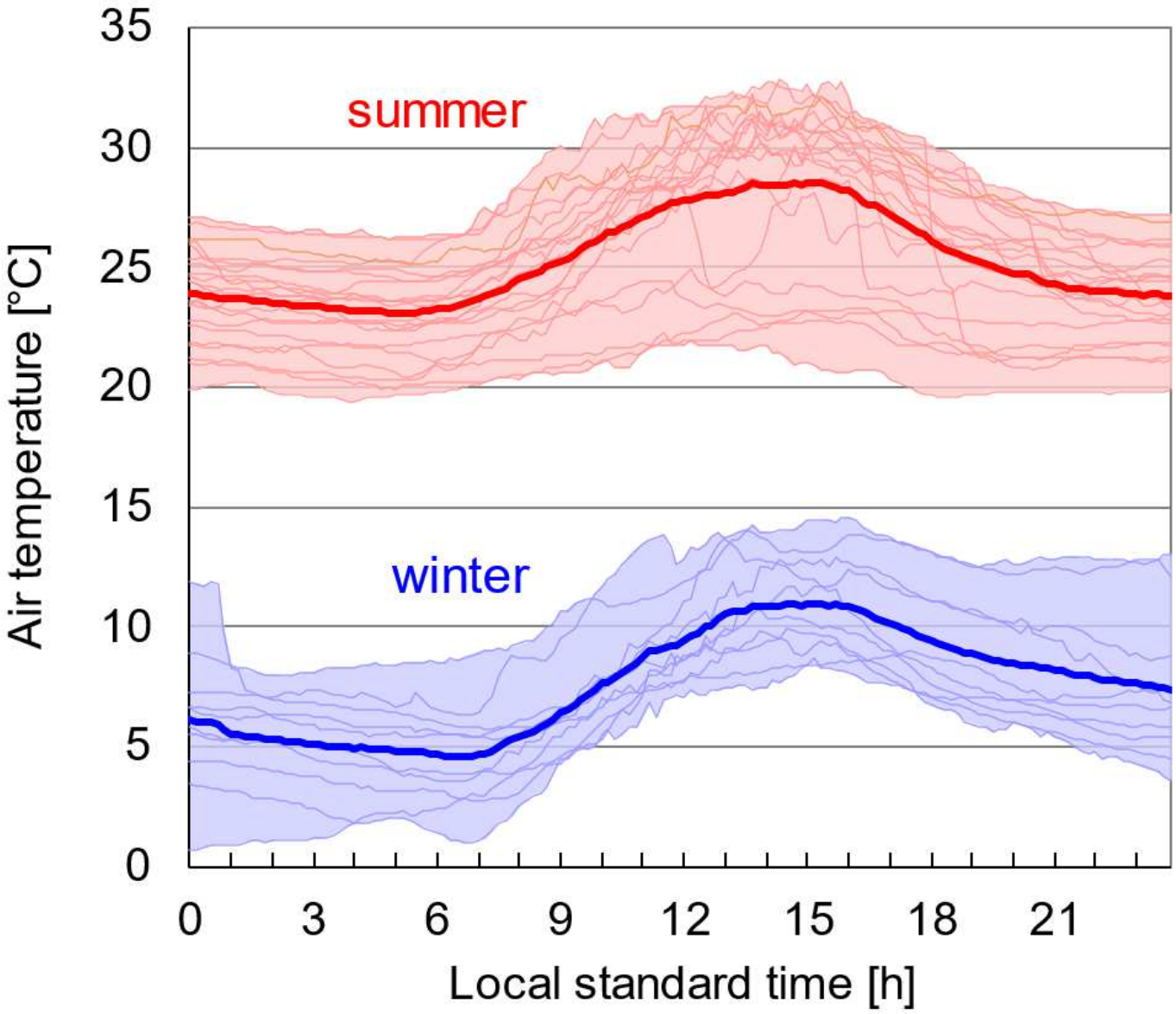

Figure 6

Observed air temperatures on the roof of the target building. For each observation period, the shaded area shows the full ranges of observed values with the thick line indicating average values

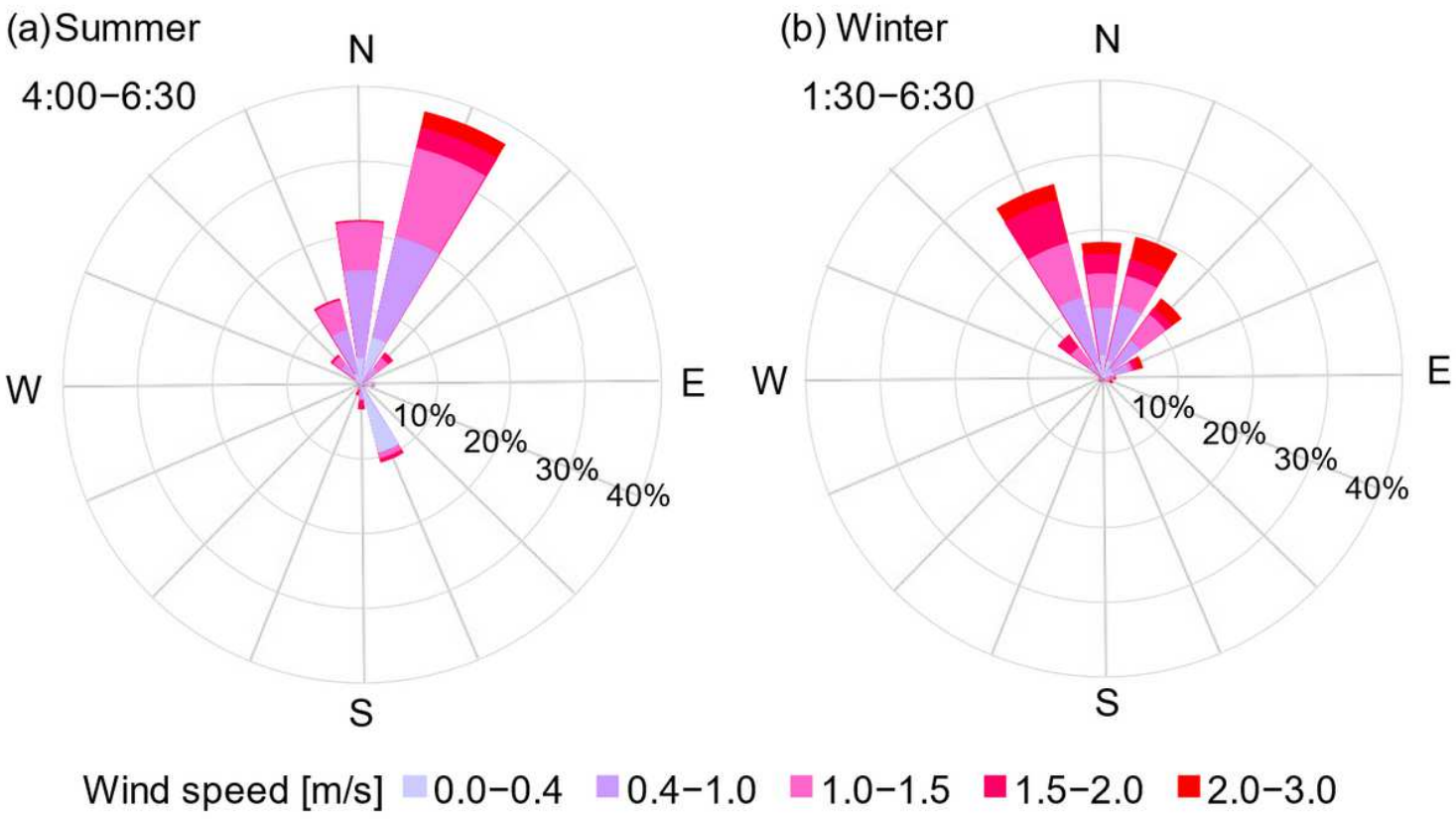

Figure 7

Wind rose for the operation times of ASHPWH during each observation period: (a) summer (4:00–6:30 am) and (b) winter (1:30–6:30 am)

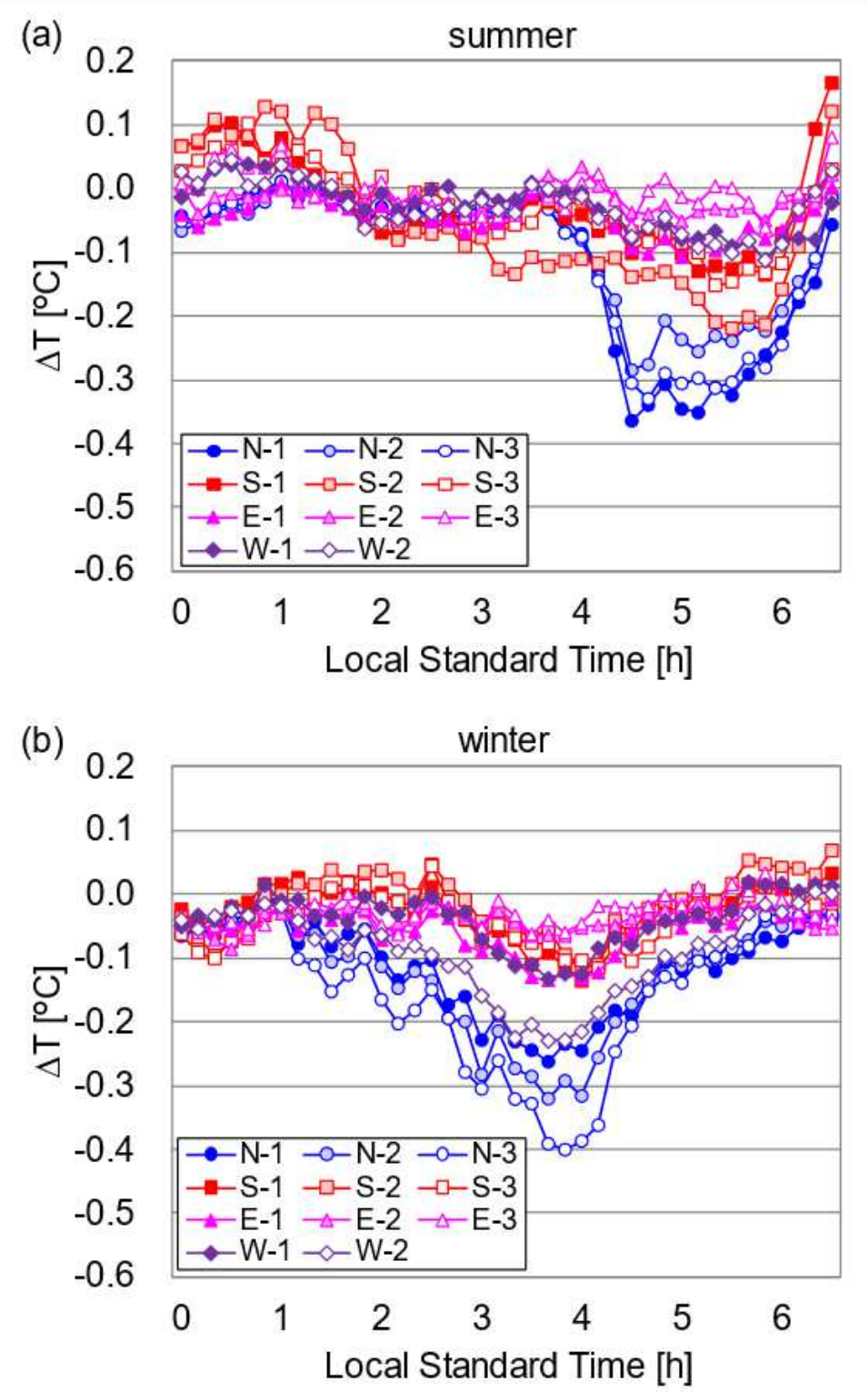

Figure 8

Average effect of cold exhaust on average 1.5-m air temperatures (ΔT) at each measurement point for each observation period: (a) summer and (b) winter

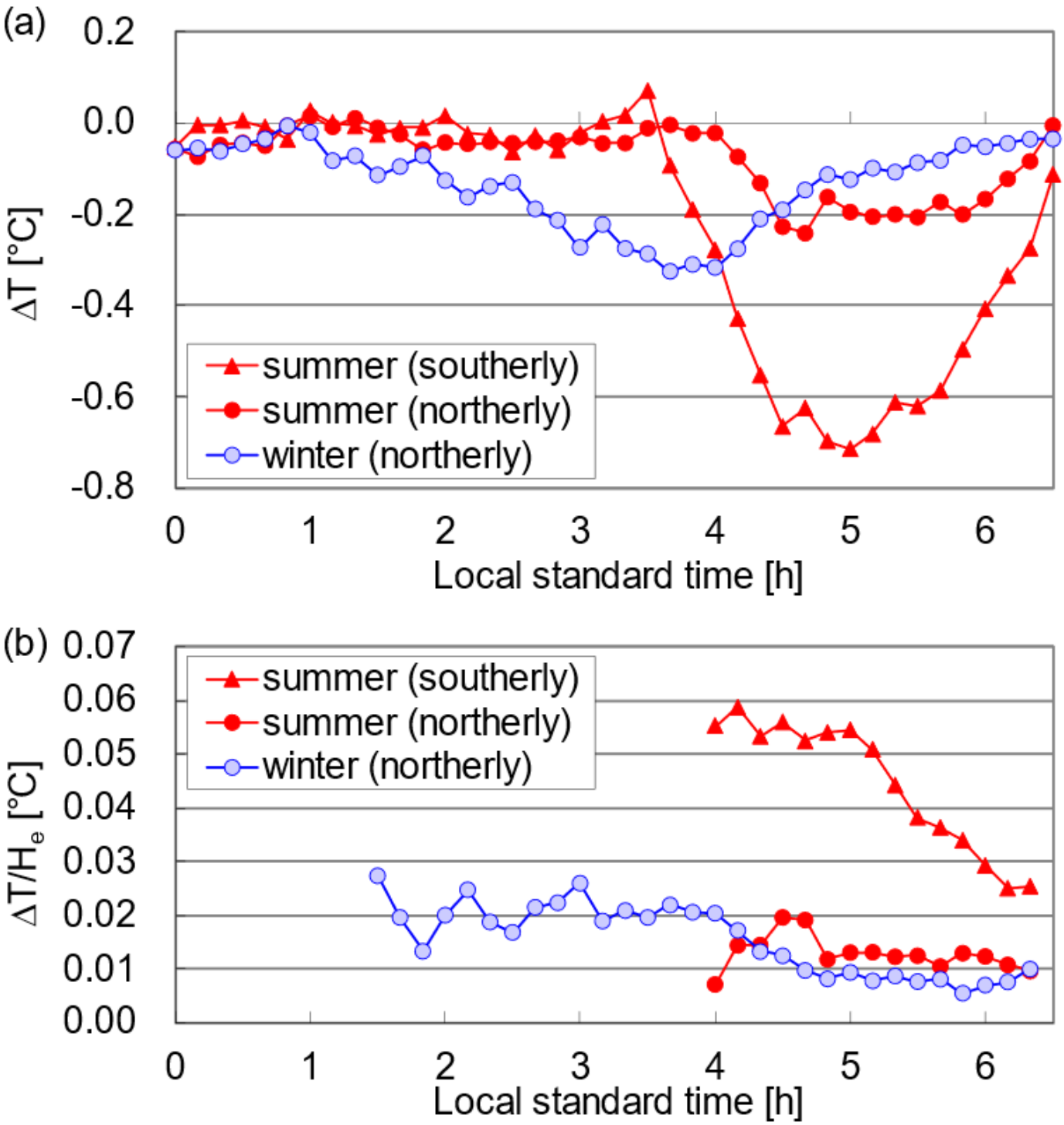

Figure 9

(a) Average of the effect of cold exhaust on air temperatures (ΔT) at three measurement points (N-1, N-2, and N-3) on the northern side of the site (sorted by observation period and wind direction). (b) The sensitivity of temperature to cold exhaust (ΔT/He)

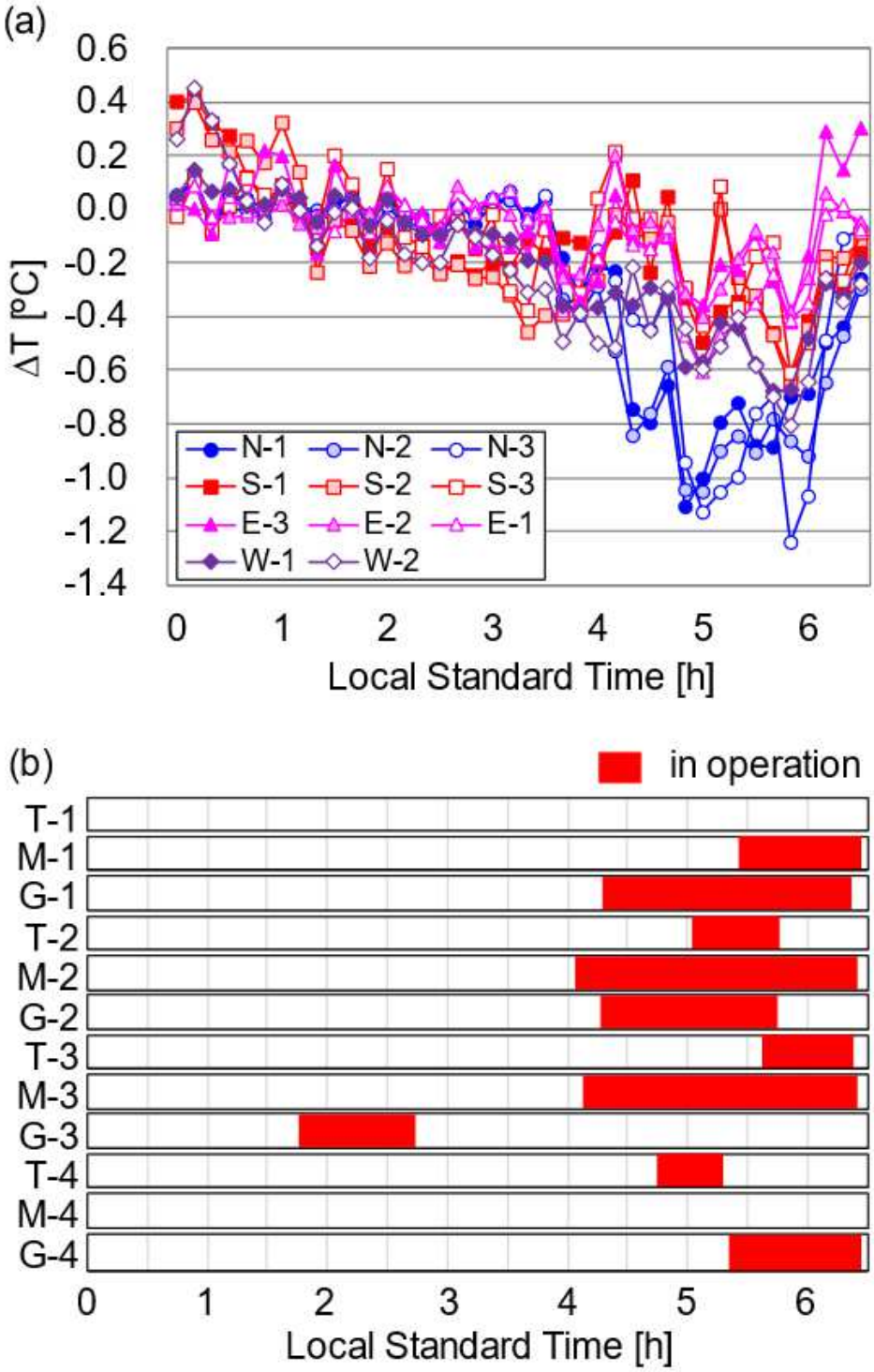

Figure 10

(a) Effect of cold exhaust on air temperatures (ΔT) observed at each measurement point of 1.5-m height; (b) operation status of each ASHPWH unit on the northern side of the building, on August 20, 2008

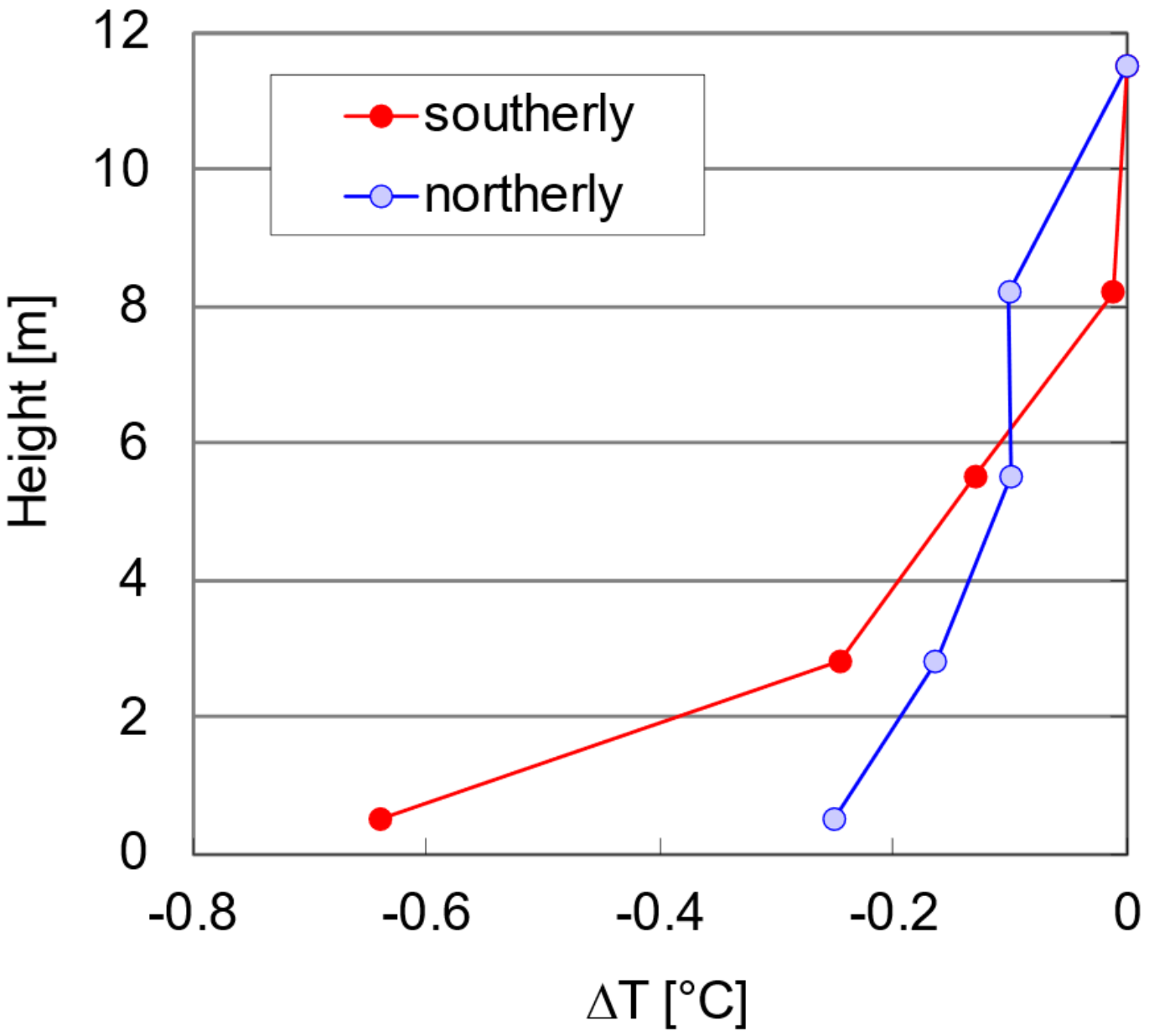

Figure 11

Vertical profile of the average effects of cold exhaust on temperature (ΔT) along the north side of the building at 5:00 am in the summer observation period (sorted by main wind direction)

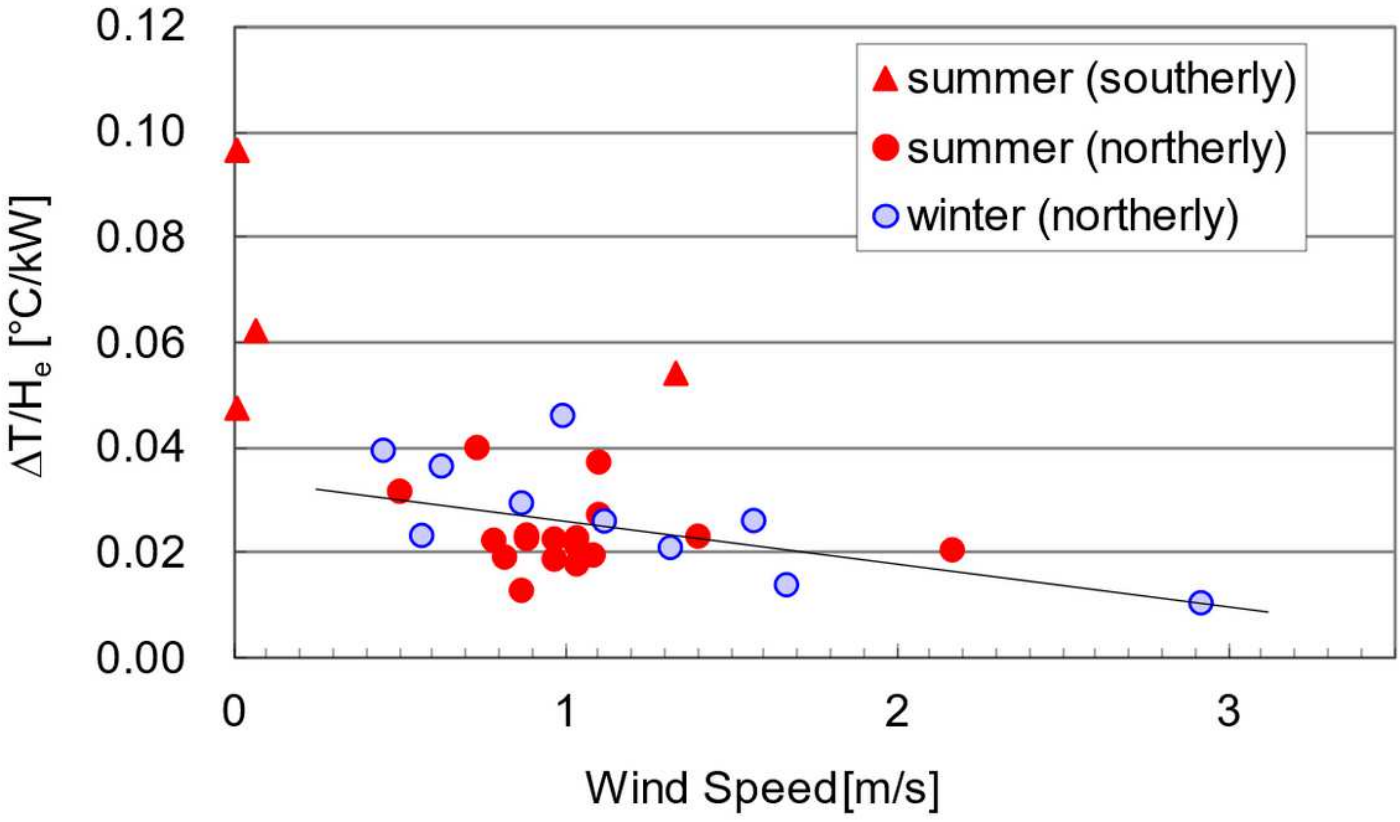

Figure 12

Relationship between the sensitivity of 1.5-m temperature to cold exhaust (ΔT/He) and wind speed. The value of ΔT is the average of those observed at points N-1, N-2, and N-3. The values of ΔT/He are a 10-min average taken at the peak time of ΔT for each day; the wind speed values are 1-h averages prior to the peak time. The straight line is a linear regression of data on days with northerly wind

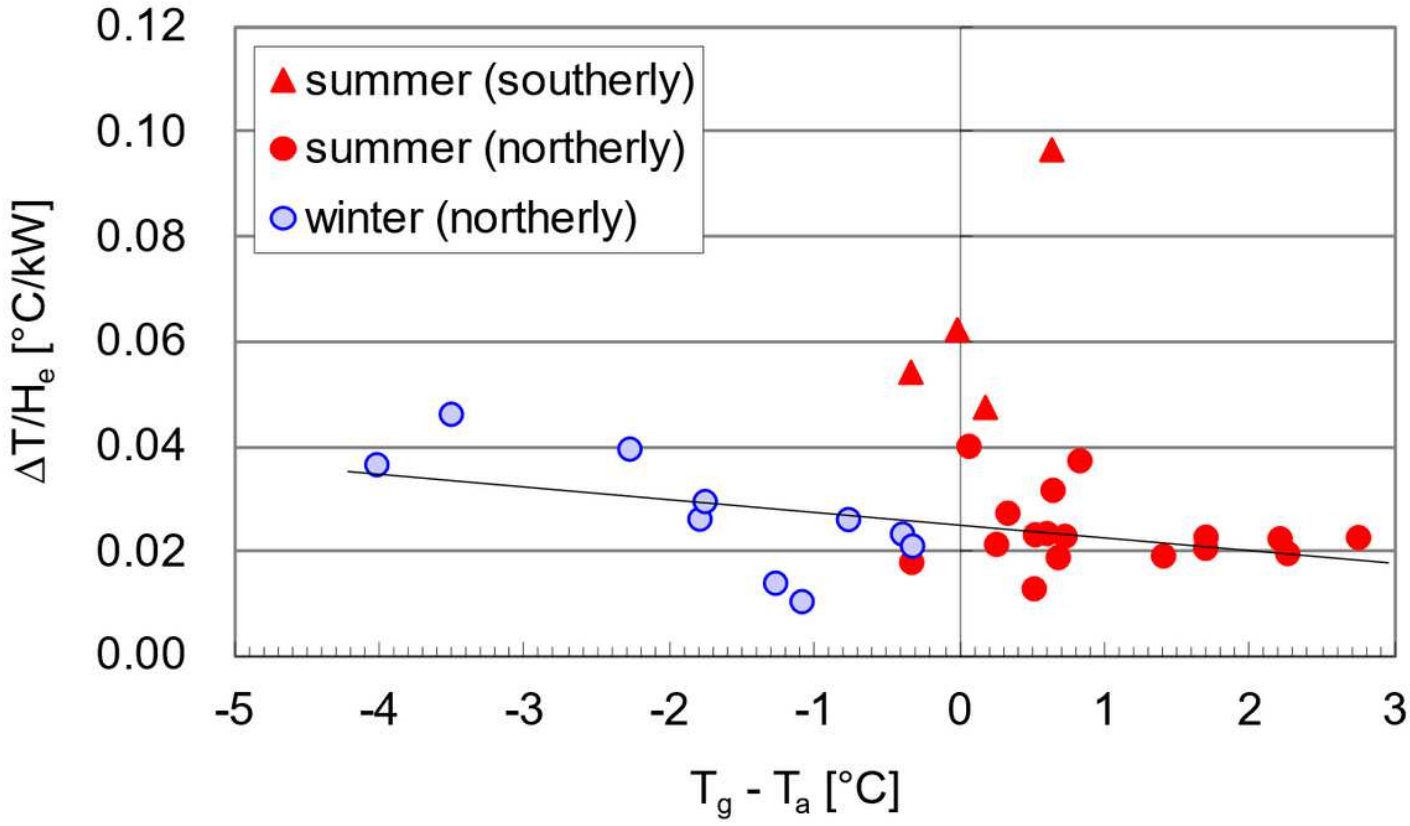

Figure 13

Same as Fig. 12, but for the difference between the air temperature and ground surface temperature (Tg−Ta; 1-hour average before peak time of ΔT) instead of the wind speed

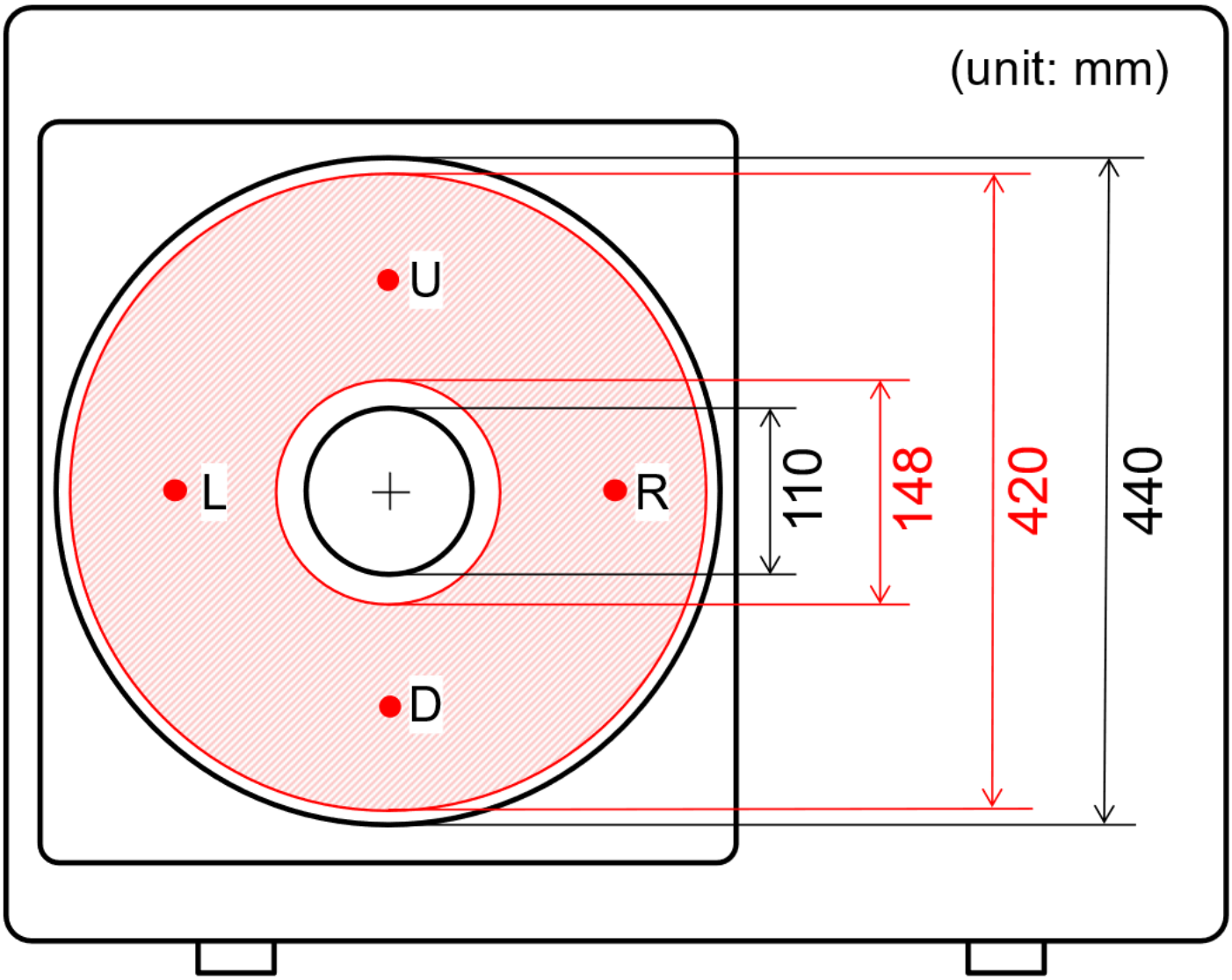

Figure 14

Measurement points of temperature and air velocity at the air outlet of the outdoor unit. The red shaded area indicates the estimated effective blowing area of the outlet

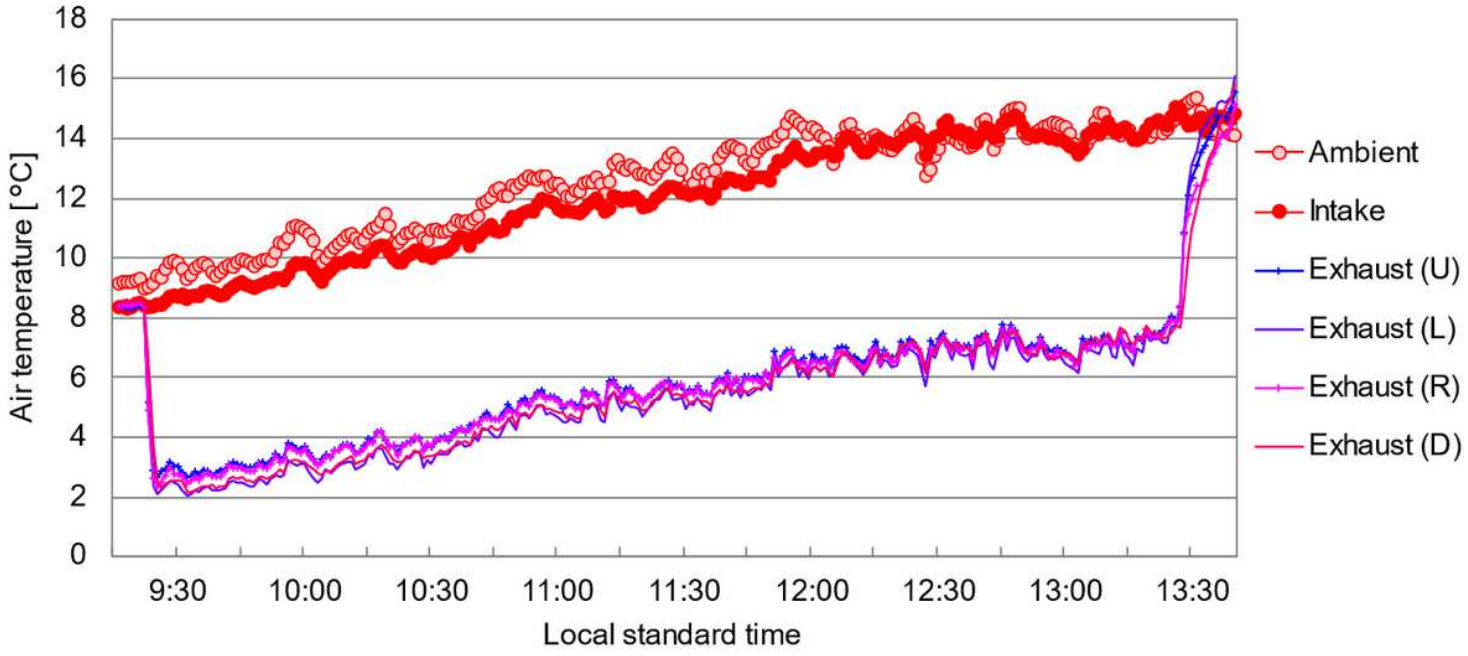

Figure 15

Time series of the temperature of the ambient air, the intake, and the exhaust of the outdoor unit. The exhaust temperatures are measured at points U, L, R, and D (indicated in Fig. 14)

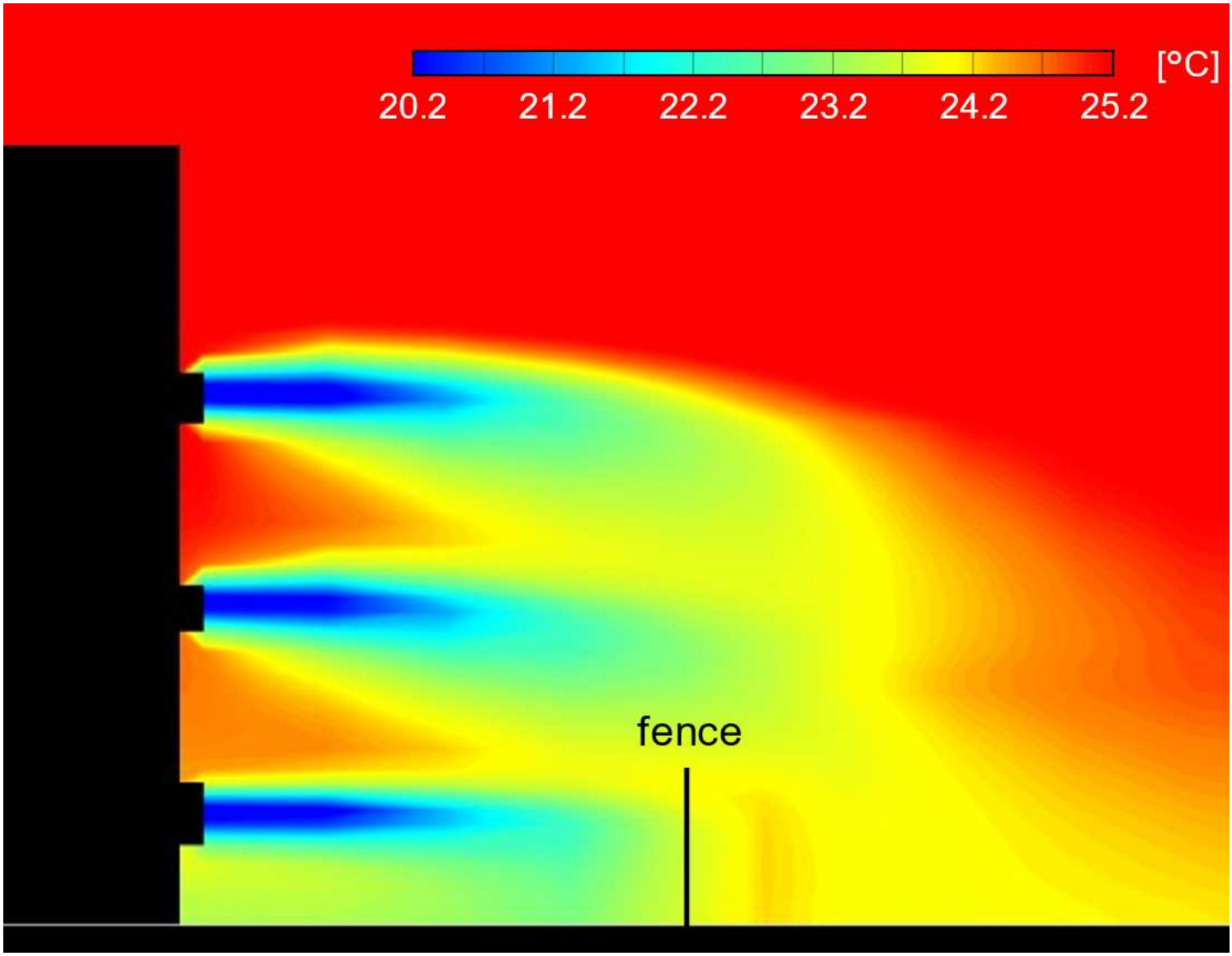

Figure 16

Simulated vertical cross section of air temperature distribution along cold exhaust outlets

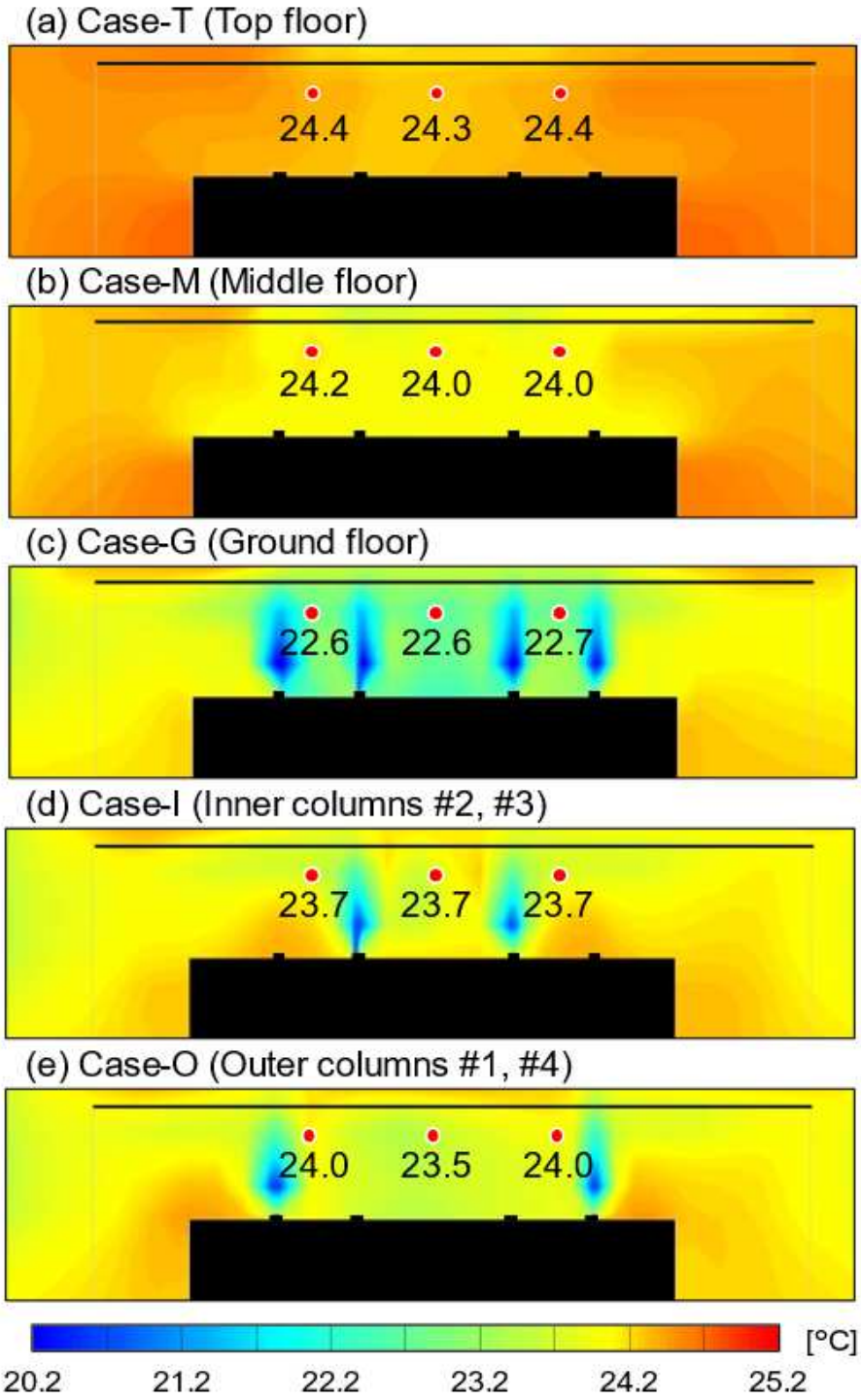

Figure 17

Simulated horizontal distribution of 1.5-m air temperature on the northern side of the site for cases (a) T, (b) M (c) G, (d) I, and (e) O. The red circles indicate the N-1, N-2, and N-3 measurement points

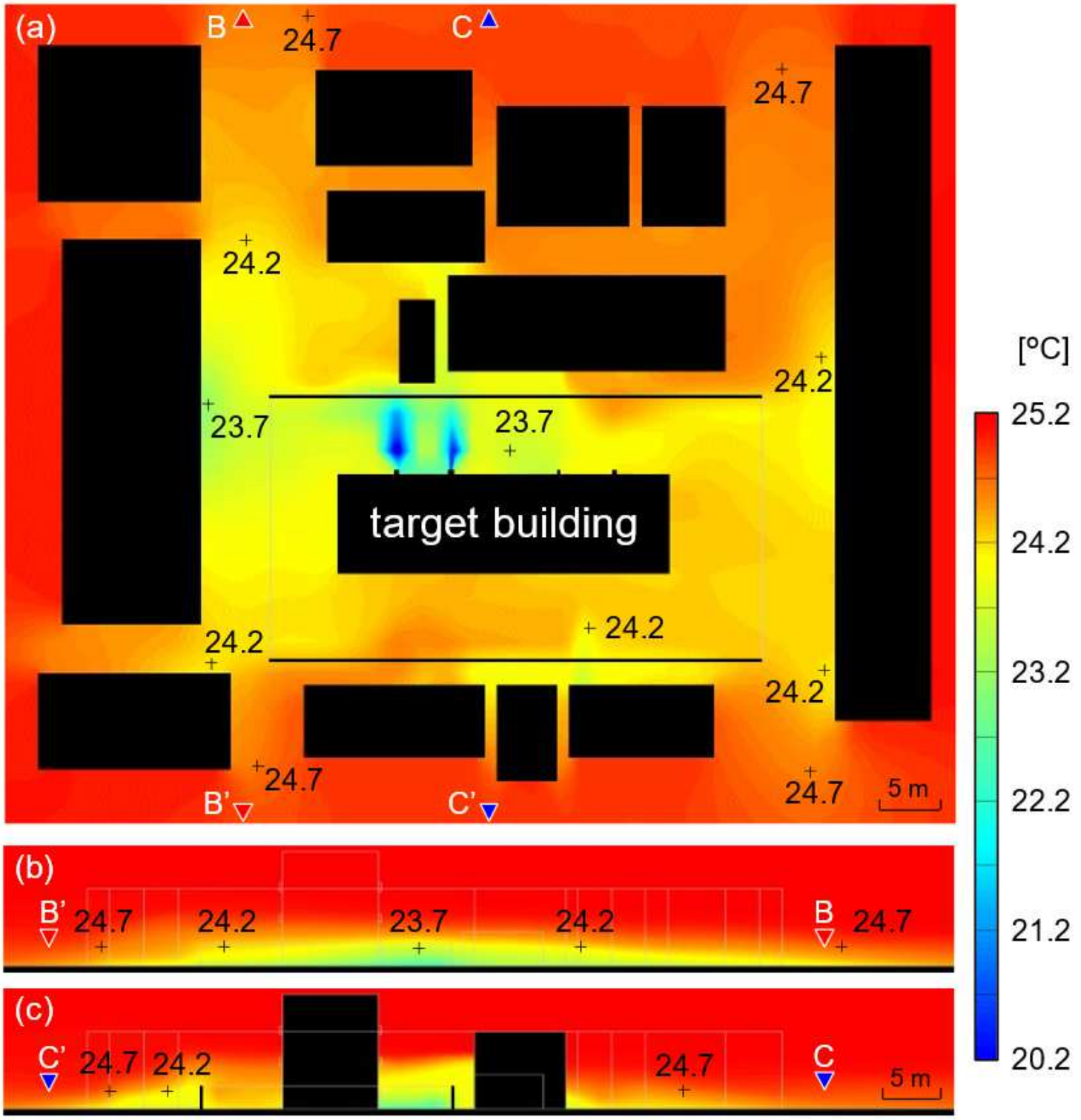

Figure 18

Simulated distribution of air temperature at 5:00 am on August 20, 2008: (a) horizontal distribution 1.5 m above the ground, (b) vertical cross section along north-south line BB', and (c) same as (b), but for line CC'